ARTICLES

Chalcone-Analogue Dyes Emitting in the Near-Infrared (NIR): Influence of Donor−Acceptor Substitution and Cation Complexation on Their Spectroscopic Properties and X-ray Structure

Knut Rurack,*,†,‡ Julia L. Bricks,§ Günter Reck,‡ Reiner Radeglia,‡ and Ute Resch-Genger‡

Institut für Physikalische und Theoretische Chemie, Humboldt Universität zu Berlin, Bunsenstrasse 1, D-10117 Berlin, Bundesanstalt für Materialforschung und -prüfung (BAM), Richard-Willstätter-Strasse 11, D-12489 Berlin, and Institute of Organic Chemistry, National Academy of Sciences of the Ukraine, Murmanskaya 5, 253660, Kiev-94, Ukraine

Received: December 6, 1999

The photophysical properties of several newly synthesized 1-benzothiazole-3-(4-donor)-phenyl-substituted prop-2-en-1-ones (substituted chalcones) are studied as a function of solvent polarity, temperature, and metal ion by employing steady-state and time-resolved spectroscopy. To investigate the effect of bulkiness and donor strength of the anilino moiety on the spectroscopic properties of these dyes, the spectroscopic behavior of the 4-*N*-dimethylamino (DMA), the 4-*N*-tetraoxa-monoaza-15-crown-5 (A15C5), and the 4-*N*-tetrathia-monoaza-15-crown-5 ($AT_4$15C5) derivatives as well as the 3-julolidino (Jul) analogue is compared. Absorption and fluorescence measurements reveal that the strength of the intramolecular charge transfer (ICT) process increases on the order of $AT_4$15C5 < A15C5 ∼ DMA < Jul. The slight but significant differences between the two crowned dyes are well-supported by the results of the X-ray structure analysis, where oxa aza and thia aza crowns show essentially different geometries. For both fluoroionophores, this variation of heteroatom substitution pattern of the receptor induces specific cation selectivities. The spectroscopic effects accompanying complexation and the different binding sites are studied by steady-state and time-resolved optical spectroscopy as well as NMR spectroscopy. Whereas the probe carrying a tetraoxa monoaza 15-crown-5 receptor shows cation-induced fluorescence enhancement in the presence of alkali and alkaline-earth metal ions, its tetrathia analogue binds selectively to Hg^{II}, Ag^{I}, and Cu^{II} in acetonitrile. Moreover, an increase in fluorescence is observed for the latter probe even upon coordination to the widely known fluorescence quencher Hg^{II}. Besides receptor complexation, chelate formation in the benzothiazole-carbonyl acceptor part of these intrinsic fluorescent probes is possible, leading to a chromoionophoric signaling behavior in the near-infrared (NIR).

1. Introduction

Fluorescent dyes that absorb and emit in the visible (vis) and/or near-infrared (NIR) are of major interest in many fields of dye chemistry such as, e.g., development of luminescent pigments for plastics and fibers or fluoroionophore design for (bio)chemical or environmental analysis.[1−3] In the latter case, interfering background fluorescence from inorganic or organic matter (matrix autofluorescence) can be minimized by employing fluorescent sensor molecules that emit at wavelengths above 600 nm, thus allowing a spectral discrimination of this autofluorescence.

In the field of chemical analysis, especially fluorometric metal ion detection in various media such as wastewater, body fluids, or rivers and lakes has received much interest lately.[2−4] The detection of these usually nonfluorescent analytes with fluorometry, a very sensitive and nondestructive analytical method, is commonly realized by employing ion sensitive organic sensor molecules (fluorescent probes) that undergo changes in their absorption and/or emission properties upon metal ion binding.[3,5] The most commonly employed and well-suited fluorescent probes are modular systems where the cation selective receptor is either covalently attached to the fluorophore through an alkyl spacer or is an integral part of the chromophore π-electron system.[5] In the former case, complexation of the receptor to a cation is accompanied by a change in fluorescence intensity due to complexation-induced inhibition of a nonradiative process, typically a photoinduced electron transfer (PET) process.[6] For the latter systems, both spectral and intensity changes of the fluorophore emission occur upon cation complexation, the observed effects ideally being cation specific.[5,7] These intrinsic probes are usually designed as donor−acceptor-substituted π-systems, and their excited-state behavior is usually governed by an intramolecular charge transfer (ICT) process. In most cases, the cation receptor is located in the donor part of the molecule.[7] Thus, the optical properties of these ICT probes are strongly solvent-dependent and the fluorescence observed under many analytic conditions, i.e., in polar liquid media, is largely Stokes-shifted. Coordination to the nitrogen donor atom

† Humboldt Universität zu Berlin.
‡ Bundesanstalt für Materialforschung und -prüfung.
§ National Academy of Sciences of the Ukraine.

10.1021/jp994269k CCC: $19.00
Published on Web 03/17/2000

SCHEME 1: Chemical Structures and Labeling of the Compounds Investigated

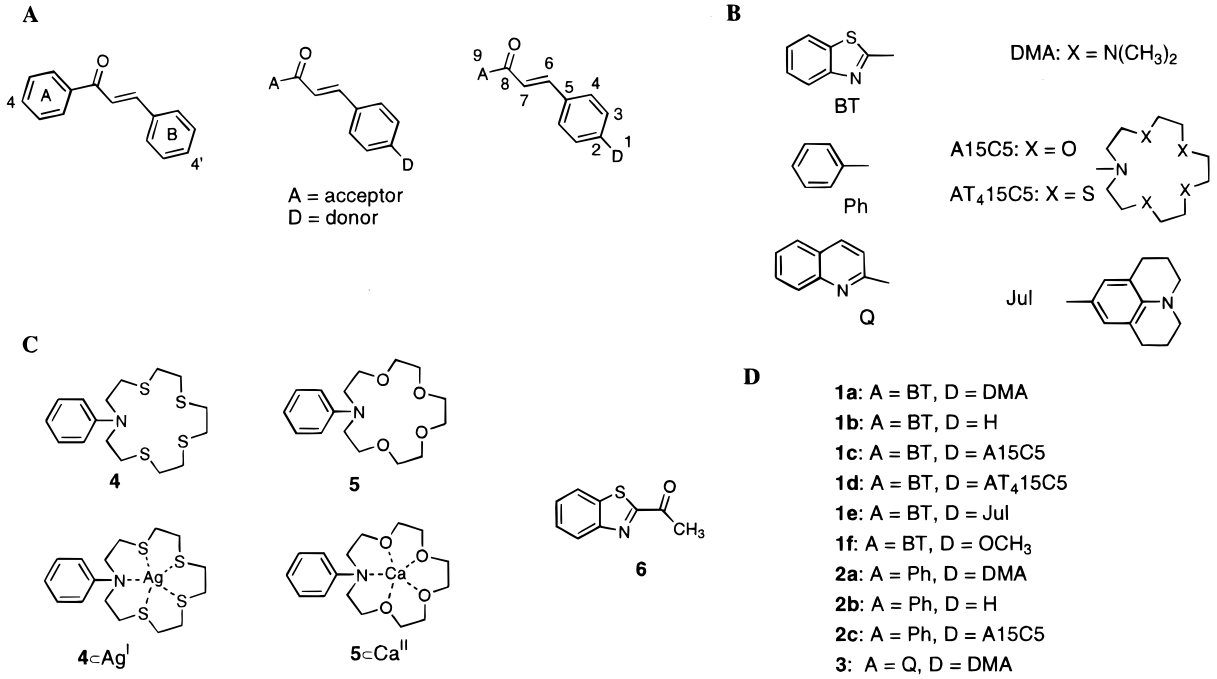

of the receptor of an ICT probe often leads to pronounced spectral shifts in both absorption and emission but only small changes in fluorescence intensity and lifetime are found, often entailing cation-induced fluorescence quenching or comparatively small fluorescence enhancement factors (FEF of ca. 2−5).[5,7,8] Moreover, although the origin of the complexation-induced spectral effects (size and direction of the shift) is partly understood,[5,7,9−13] the mechanisms governing fluorescence enhancement or quenching in these ICT probes are still under discussion. Concerning the analytes of interest, the majority of fluoroionophores have been designed for alkali and alkaline-earth metal ions (for some examples, see refs 6, 7, and 14−20) and only a comparatively small number of modular fluorescent probes is so far known for heavy and transition metal ions (ICT probes, refs 21−28; PET probes, refs 29−31).

The cation selectivity of these modular fluoroionophores is to a large extent controlled by the specificity of the receptor. The great majority of these systems were designed for s-block alkali and alkaline-earth metal ions, which are classified as "hard" cations by Pearson's concept of "hard and soft acids and bases" (HSAB).[32,33] Thus, the corresponding fluorescent probes typically contain macrocycles with "hard" oxygen atoms such as crown ethers or their monoaza analogues as cation specific receptors. Substitution of two oxygen atoms of the crown ether for "soft" nitrogen atoms yields macrocyclic amino polyethers that, besides forming complexes with alkali and alkaline-earth metal ions, have been reported to also bind heavy metal ions.[14,22,25,26] However, complexation of heavy metal ions by these diaza crowns is rather nonselective.[34,35]

The design of selective fluorescent probes for soft heavy and transition metal ions requires the use of macrocyclic or acyclic ligands in which some or all of the "hard" oxygen atoms are replaced by "soft" sulfur and/or nitrogen atoms. Besides their greater selectivity for thiophilic heavy and transition metal ions and the fact that alkali and alkaline-earth metal ions are not expected to interfere in cation complexation,[35,36] the system thia aza crown/transition metal ion also shows considerably higher cation binding constants as compared to the system oxa aza crown/alkali or alkaline-earth metal ion and should thus permit lower detection limits. Only recently were some examples for chromo-[37] and fluoroionophores reported,[24,27,28,31] which contain the heteroatoms sulfur and nitrogen or oxygen as cation coordination sites in the macrocyclic receptor part of the molecule. However, in most cases (e.g., refs 30 and 31), the fluorophore emission is completely quenched upon binding to paramagnetic or heavy metal ions due to enhanced spin−orbit coupling, energy, or electron transfer.[38−40]

The class of dyes investigated here, donor−acceptor-substituted (D−A-) chalcones (general chemical structure shown in Scheme 1A),[41] was chosen by us because their derivatives with an annelated heteroaromatic acceptor (e.g., benzothiazole) and a nitrogen containing donor show analytically valuable spectroscopic properties, i.e., an intensive absorption band at ≥450 nm and a strongly Stokes-shifted NIR emission in solvents of high polarity. Moreover, since tuning of chalcones by exchanging donor and acceptor moieties is synthetically feasible, this feature allowed the construction of new fluoroionophores with special attention being directed toward ion discrimination on the basis of carefully directed receptor design. Chalcones are well-known precursors of many naturally occurring pigments as, e.g., their (poly)hydroxylated derivatives or flavones,[42] and they are used in various fields of application such as, for instance, for UV-absorption filters in polymers,[43] in different kinds of optical materials,[44] in food technology,[45] and in medical therapy.[46]

The photophysical properties of substituted chalcones have been studied by numerous researchers involving mostly asymmetrical D−A-chalcones and to a minor extent symmetrical D−A−D-chalcones.[47−58] Whereas in the former case, the acceptor is usually exemplified by a 4-substituted phenyl derivative (A = Ph, Scheme 1), in the latter case the carbonyl group is the acceptor part and the two 4′-donor-substituted B-rings serve as bis-donor; i.e., these molecules are of the 1,5-diphenyl-1,4-pentadien-3-one type.[48,53] Until today, only very few heteroaromatic moieties have been introduced into the acceptor part of these chalcones.[48]

To get a more fundamental understanding of the mechanisms governing the spectroscopic behavior of the unbound as well as the complexed chalcone-type fluorescent probes, we inves-

tigated the intramolecular charge transfer (ICT) process and photophysical properties of the crowned D−A-chalcones **1c**, **1d**, and **2c** and their model compounds **1a**, **1b**, **1e**, **1f**, **2a**, **2b**, and **3** (Scheme 1) as a function of solvent polarity, temperature, and metal ion employing steady-state and time-resolved spectroscopy. The sensing abilities of the crowned derivatives and the possibilities in ion discrimination by the choice of an appropriate receptor (tetrathia monoaza 15-crown-5 vs tetraoxa monoaza 15-crown-5) were studied in acetonitrile and involve the alkali and alkaline-earth metal ions Li^{I}, Na^{I}, K^{I}, Mg^{II}, Ca^{II}, Sr^{II}, and Ba^{II} as well as the heavy and transition metal ions Ag^{I}, Cu^{I}, Cu^{II}, Ni^{II}, Co^{II}, Zn^{II}, Cd^{II}, Hg^{II}, and Pb^{II}. Besides a comparison with the model compounds, some of the complexes are studied by NMR spectroscopy to determine their actual coordination sites. Since **1d** is among the first examples for fluorescent probes carrying the tetrathia monoaza 15-crown-5 ($AT_4$15C5) ion-responsive receptor,[27,28] **1c** and **1d**, the separate receptor units *N*-phenyl-$AT_4$15C5 (**4**) and *N*-phenyl-tetraoxa-monoaza-15-crown-5 (Ph-A15C5, **5**), as well as the complexes **4**⊂Ag^{I} and **5**⊂Ca^{II} were additionally investigated by X-ray structure analysis to elucidate the impact of different monoaza crown ether receptors on the molecular properties of this type of dye.

2. Experimental Section[59]

2.1. Materials. The starting materials for the syntheses were obtained from Aldrich and Merck. All the solvents employed were of UV-spectroscopic grade and purchased from Aldrich. The following abbreviations are used throughout the text: methanol, MeOH; ethanol, EtOH; isopropanol, PrOH; ethylene glycol, EG; acetonitrile, MeCN; dichloromethane, CH_2Cl_2; diethyl ether, Et_2O; 1,4-dioxane, Diox; *n*-hexane, Hex. Metal perchlorates and CuCl purchased from Merck, Acros, and Aldrich were of highest purity available and dried in a vacuum oven before use.[60] For the determination of the complex stability constants, acetonitrile was distilled from CaH_2 prior to use.

2.2. Synthesis—General Methods. The chemical structures of the synthesized compounds were confirmed by elemental analysis, ^{1}H NMR, ^{13}C NMR, IR, and MS, and their purity was checked by reversed-phase HPLC (HPLC setup from Merck-Hitachi; RP18 column; acetonitrile/water = 75/25 as eluent) employing UV detection (UV detector from Knaur; fixed wavelength at 310 nm). NMR spectra were obtained with a 500 MHz NMR spectrometer Varian Unity$_{plus}$ 500. The IR spectra were measured with a Bruker FTIR spectrometer IFS66v. The mass spectra were recorded on a Finnigan MAT 95 spectrometer with an ESI-II/APCI-Source for electrospray ionization and the base peaks $[M + Na]^+$ were determined. The melting points (mp) measured with a digital melting point analyzer IA 9100 (Kleinfeld GmbH) are uncorrected. Descriptions of the syntheses and analytical data are provided in the Supporting Information, section S1.

2.3. Steady-State Absorption and Fluorescence Spectroscopy.[61] UV/vis spectra were recorded on a Carl−Zeiss Specord M400/M500 absorption spectrometer. Only for the temperature-dependent absorption experiments was a Bruins Instruments Omega 10 spectrophotometer employed. Steady-state emission spectra were recorded on a Perkin-Elmer LS50B and a Spectronics Instruments 8100 spectrofluorometer. For the fluorescence experiments, only dilute solutions with an optical density (OD) below 0.01 at the excitation wavelength (OD < 0.04 at the absorption maximum) were used. All the fluorescence spectra presented here are corrected, and the relative fluorescence quantum yields (ϕ_f) were determined by comparison with the fluorescence standards fluorescein 27, quinine sulfate, coumarin 1, and DCM.[62] The uncertainties of the measurement were determined to ±5% (for $\phi_f > 0.2$), ±10% (for $0.2 > \phi_f > 0.02$), ±20% (for $0.02 > \phi_f > 5 \times 10^{-3}$), and ±30% (for $5 \times 10^{-3} > \phi_f$), respectively. Details on quantum yield determination and instrument correction are given in the Supporting Information, section S3.

2.4. Time-Resolved Fluorescence Spectroscopy.[61] Fluorescence lifetimes (τ_f) were measured employing a unique laser impulse fluorometer with picosecond time resolution described elsewhere.[63] The sample was excited with the second or third harmonic output (LBO crystal or sum frequency of the ground wave and the second harmonic generated in a BBO crystal) of a regenerative mode-locked argon ion laser-pumped Ti:sapphire laser at a repetition rate of either 82 or 4 MHz (reduction by synchronized pulse selection). The fluorescence was collected at right angles (emission polarizer set at 54.7°; monochromator with spectral bandwidths of 4, 8, and 16 nm) and the fluorescence decays were recorded with a time-correlated single photon counting setup and a time division of 5.2 ps channel^{-1} (82/4 MHz version) or 52.6 ps channel^{-1} (4 MHz version). The corresponding experimental accuracies were ±3 ps and ±0.04 ns, respectively. The laser beam was attenuated using a double prism attenuator from LTB, and typical excitation energies were in the nanowatt to microwatt range (average laser power). The instrumental response function (IRF) of the system was typically 30 ps (full width at half-maximum). Further details on the calibration of the instrument are provided in the Supporting Information, section S4.

The fluorescence decay profiles were analyzed with a PC using the software packages IBH Decay Analysis Software V4.2 (IBH Consultants Ltd.) and Global Unlimited V2.2 (Laboratory for Fluorescence Dynamics, University of Illinois), respectively. The accuracy of the fit of the single decays, as judged by reduced χ^2 (χ_R^2), the autocorrelation function *C(j)* of the residuals, and the Durbin−Watson parameter (DW), was always acceptable, yielding values of $\chi_R^2 < 1.2$ and DW > 1.8. Global analysis of the decays recorded at different emission wavelengths implies that the decay times of the species are linked, while the program varies the preexponential factors and lifetimes until the changes in the error surface (χ^2 surface) are minimal, i.e., until convergence is reached. The fitting results are judged for every single decay (local χ_R^2) and for all the decays (global χ_R^2), respectively. Except as otherwise indicated, the errors for all the measurements presented here were below a global $\chi_R^2 = 1.2$.

2.5. NMR Spectroscopy. One and two-dimensional NMR spectra (COSY (90°) and ^{1}H/^{13}C−HECTOR) were measured using a Bruker spectrometer DMX 400 (5 mm tube, CD_3CN, deuterium lock). In all the cases, the solvent employed was deuterated acetonitrile. For the complexation experiments, cations were added in a 180-fold excess (dye concentration $c_L = 1.5 \times 10^{-3}$ M).[64]

2.6. Complex Stability Constants Determined by Steady-State Spectroscopy. The complex stability constants K_S reported here were determined from both absorption (in 50 or 100 mm absorption cells) and fluorescence measurements (in 10 mm quartz cells) and were measured by titrating a dilute solution of the ligand (typically 10^{-6} M) by adding aliquots of metal ion solution (c_{M0} titration). For fitting of the complexometric titration data, the following equations apply (X = absorption or fluorescence intensity; a, b = constants; c_M, c_L, c_{ML} = free metal, free ligand, and complex concentrations, c_{Y0} = total concentrations) and the theoretical background is discussed in more detail in refs 16 and 65.

$$K_S = \frac{c_{ML}}{c_L c_M} \quad (1)$$

$$X_0 = ac_{L0}, \qquad X_{lim} = bc_{L0}, \qquad \text{and} \qquad X = ac_L + bc_M \quad (2)$$

$$c_{L0} = c_L + c_{ML} \qquad \text{and} \qquad c_{M0} = c_M + c_{ML} \quad (3)$$

Combination allows for the graphical determination of K_S according to eq 4 (when X_{lim} is not known). For strong complexation, when $c_M \sim c_{M0}$ is not valid anymore, eq 5 can be derived from eqs 1−3.[16,65]

$$\frac{X_0}{X - X_0} = \frac{a}{b - a}\frac{1}{K_S c_M} + 1 \quad (4)$$

$$X = X_0 + \frac{X_{lim} - X_0}{2c_{L0}}\left\{c_{L0} + c_{M0} + \frac{1}{K_S} - \left[\left(c_{L0} + c_{M0} + \frac{1}{K_S}\right)^2 - 4c_{L0}c_{M0}\right]^{1/2}\right\} \quad (5)$$

The reported values are mean values of at least two measurements with correlation coefficients >0.99.[66]

2.7. X-ray Structure Analysis. The X-ray data of **1c**, **1d**, **4**, and **4**⊂Ag^I were collected on an Enraf-Nonius CAD-4 diffractometer at 293 K using Mo Kα radiation (λ = 0.710 73 Å) monochromatized by a graphite crystal. The structures were solved by direct methods and refined by full-matrix least squares calculations (Enraf-Nonius MOLEN). X-ray data collection of **5** and **5**⊂Ca^{II} was carried out on a Siemens SMART diffractometer under similar conditions as described for **1c**, **1d**, **4**, and **4**⊂Ag^I. Structure solution using direct methods and full-matrix least-squares refinement were performed with SHELXTL. The hydrogen atoms of all the structures were introduced in their calculated positions and refined using riding models.[67]

3. Results and Discussion

3.1. X-ray Crystallography. The total X-ray structures of the four molecules in the uncomplexed state and the two complexes **4**⊂Ag^I and **5**⊂Ca^{II} are collected in Figure 1. Whereas for the tetraoxa monoaza 15-crown-5 (A15C5)-substituted compounds the phenyl group is in an axial position to the crown, the equatorial conformation is favored for the tetrathia monoaza 15-crown-5 ($AT_4$15C5) containing dyes. Furthermore, for **1d** two conformations **1d**(**A**) and 1**d**(**B**) are found the differences being manifested only in the substituted anilino donor unit (Figure 1 and Table 1). The close similarity between **1d** (**A** and **B**) and **4** (flat stretched conformation of the molecules) on the one and **1c** and **5** (conformation of "L"-type) on the other side is remarkable (Figure 1). The larger chromophoric unit in **1c** and **1d** barely influences the conformation of the crown ether receptor in the crystalline state. Comparing the structures of **4**⊂Ag^I and **5**⊂Ca^{II} in Figure 1 the influence of the conformation on the structure of the resulting complex is apparent. The "L"-type structure is retained in **5**⊂Ca^{II} and a mononuclear complex is formed but for **4**⊂Ag^I, a binuclear complex is found (Figure 1).

It is interesting to note that the ring conformations of the $AT_4$15C5-substituted derivatives **1d** and **4** are very similar despite a different packing of the molecules in the crystal (cf. the endocyclic torsion angles in Figure S1). Most probably this effect is due to the larger space required by the sulfur atoms compared to the oxygen atoms.

Besides the actual conformation of the chromophore and crown subunit at the anilino crown ether nitrogen atom N(1), which represents the donor atom in a donor−acceptor-substituted ICT probe, the pyramidalization at this atom is important for the degree of conjugation of the nitrogen's lone electron pair and the π-system of the phenyl ring. Here, the bond lengths between N(1) and C(16) are similar to bond lengths in peptide bonds, i.e., between 1.36 and 1.40 Å (average value of 1.37 Å, Table 1). In all the cases, the sum of the dihedral angles at N(1) equals ca. 360° (Table 1) indicating that a sp^2-like hybridization is present in the molecules and the lone electron pair is in conjugation with the short N(1)−C(16) bond. The only deviation is seen for **1d**(**B**) where all the angles equal 357.3°. Here, the conjugation can be reduced with the lone electron pair being directed "downwards" from the molecular plane. The sp^2-hybridization results in torsional angles of ca. 0° around the N(1)−C(16) bond; i.e., the chromophoric system is planar in these molecules.

In contrast, complexation leads to a rehybridization and N(1) is found to be sp^3-hybridized. Accordingly, the bond N(1)−C(16) is lengthened and amounts to 1.46 Å in both complexes studied. Moreover, the sums of the dihedral angles at N(1) are considerably reduced to 333.8° (**5**⊂Ca^{II}) and 336.2° (for **4**⊂Ag^I, Table 1) and bond lengths N(1)−M^{n+} of 2.591 Å (for **4**⊂Ag^I) and 2.724 Å (**5**⊂Ca^{II}) are found. These data are in good agreement with results published by Jonker et al. and Heijdenrijk et al. on Ba^{II} and Ag^I complexes of MAP-A15C5 derivatives (Scheme 2).[25,68,69] For **4**⊂Ag^I and **5**⊂Ca^{II}, the good fit of ion-into-the-cavity is stressed by the nearly ideal sp^3-hybridization of N(1) which Heijdenrijk et al. only observed for MAP-A15C5-1⊂Ag^I (N(1)−Ag^I = 2.58 Å, Σ(N1) = 337°). In the case of the larger Ba^{II} ion or the sterically more demanding MAP-A15C5-2, less rehybridization was found by these researchers.[69]

3.2. Steady-State Absorption and Emission of the Dyes at 298 K. The absorption and emission spectra of some of the D−A-chalcones in selected solvents are shown in Figures 2 and 3. Tables S1 and S2 combine all the spectroscopic data. Introduction of a donor to the 4′-position leads to a strong shift of the main absorption band to lower energies and the charge transfer (CT) character of this band of the anilino donor-substituted derivatives is exemplified by a comparison of the steady-state spectra of **1a**, **1b**, and **2a** in three solvents of different polarity, shown in Figure 3.

Effect of N,N-Alkylamino Substitution. The dimethylamino-substituted compounds **1a** and **2a** and the corresponding crowned fluorescent probes **1c**, **1d**, and **2c** display rather similar spectral properties, i.e., broad absorption bands and a strongly Stokes-shifted emission band in polar solvents (Figure 2, Tables S1 and S2). As follows from a comparison of **1c** and **1d**, substitution of oxygen for sulfur in the macrocycle obviously alters the electronic character of the substituent only slightly and thus barely affects the absorption spectra (Figure 2). A similar behavior has been observed by Ishikawa et al. for 4-(dinitrophenyl)hydrazones of *N*-phenyl-A15C5 and *N*-phenyl-$AT_4$15C5.[70] As can be deduced from a comparison of the spectra in Figure 3, the intramolecular charge-transfer character (ICT from nitrogen donor of ring B to aryl-carbonyl acceptor moiety) of these dyes follows from the solvent-dependent spectral shifts in absorption and emission.[71] Both bands undergo a red shift with increasing solvent polarity, the spectral shift in fluorescence being more pronounced. This increase in Stokes shift with increasing solvent polarity indicates that the fluorescent excited singlet state(s) is (are) more strongly stabilized in polar solvents than the ground-state, thus pointing to a larger dipole moment

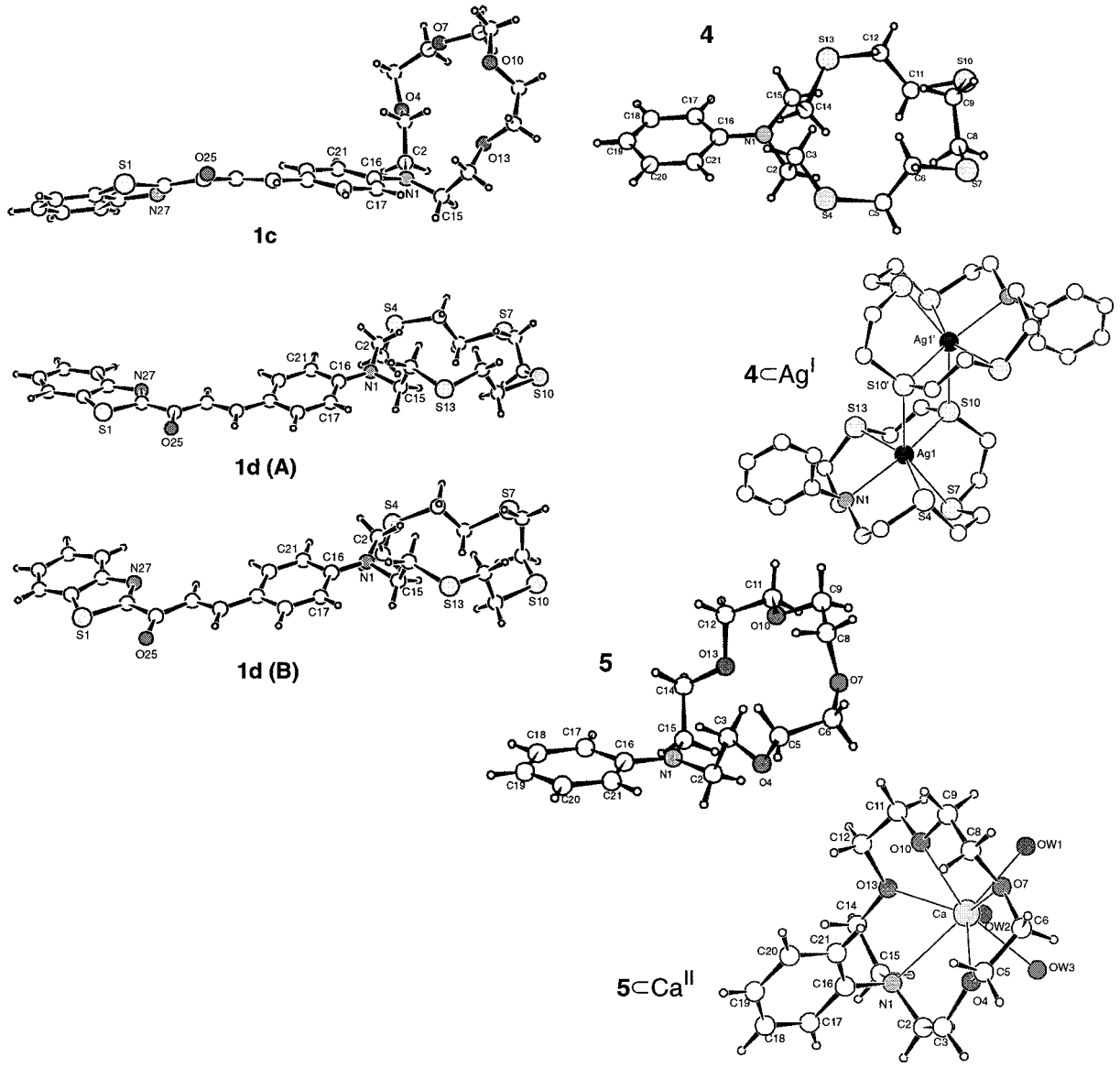

Figure 1. X-ray structures of **1c**, conformers A and B, **1d**, **4**, **5**, **4**⊂Ag^I, and **5**⊂Ca^{II}.

TABLE 1: Selected Bond Lengths (Å), Angles (deg), and Torsion Angles (deg) of 1c, 1d, 4, 5, 4⊂Ag^I, and 5⊂Ca^{II}

	1c	**1d (A)**	**1d (B)**	**4**	**5**	**4**⊂Ag^I	**5**⊂Ca^{II}
N1−C2	1.46	1.49	1.47	1.53	1.46	1.47	1.45
N1−C15	1.47	1.48	1.48	1.48	1.47	1.48	1.51
N1−C16	1.38	1.37	1.35	1.36	1.40	1.46	1.46
C2−N1−C15	118.2	115.0	112.2	116.9	118.5	111.2	113.4
C2−N1−C16	121.2	125.0	120.9	125.2	120.7	112.2	111.2
C15−N1−C16	120.7	119.6	124.2	117.8	120.7	112.8	109.2
Σ	360.1	359.6	357.3	359.9	359.9	336.2	333.8
C15−N1−C16−C17	13.6	8.8	18.5	25.1	−2.3	−52.6	120.1
C2−N1−C16−C21	10.6	15.6	3.7	21.9	1.8	−107.6	65.3

of this state as compared to the ground state.[72] Only in apolar *n*-hexane does the spectra show some vibronic structure (Figure 3).

Solvatochromic Behavior and Dipole Moments. For the *N*,*N*-alkylamino-substituted D−A-chalcone derivatives, the fluorescence excitation spectra in non H-acidic, polar solvents resemble closely the corresponding absorption spectra. In alcohols and apolar solvents such as *n*-hexane or 3-methylpentane, deviations occur. In alcohols, this behavior is also reflected by the emission spectra; i.e., measuring the emission spectrum at constantly increasing excitation wavelengths shifts the emission band to lower frequencies (e.g., in the case of **1c**, excitation at 420 and 470 nm yields bands centered at 599 and 603 nm, respectively). The behavior in apolar solvents is different. Only slight changes were detectable for fluorescence excitation and emission spectra recorded with different emission or excitation wavelengths.

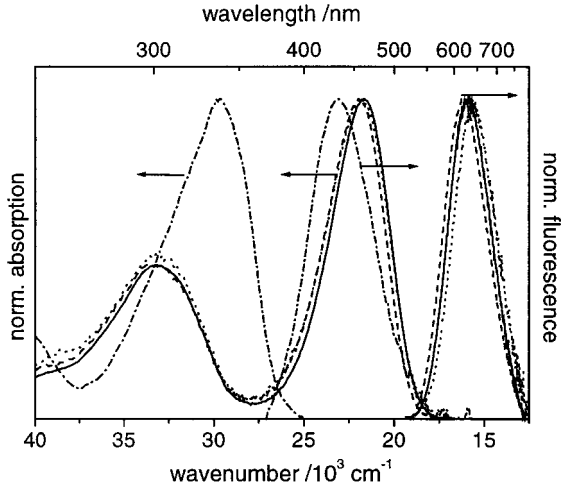

Figure 2. Normalized steady-state absorption and emission spectra of **1a** (···) **1b** (·−·−·) **1c** (—), and **1d** (---) in acetonitrile at 298 K.

SCHEME 2: Related Fluorescent Probes DCS-A15C5,[17] DCM-A15C5,[15] MAP-A15C5 Derivatives,[25] and BOZ-A15C5[65]

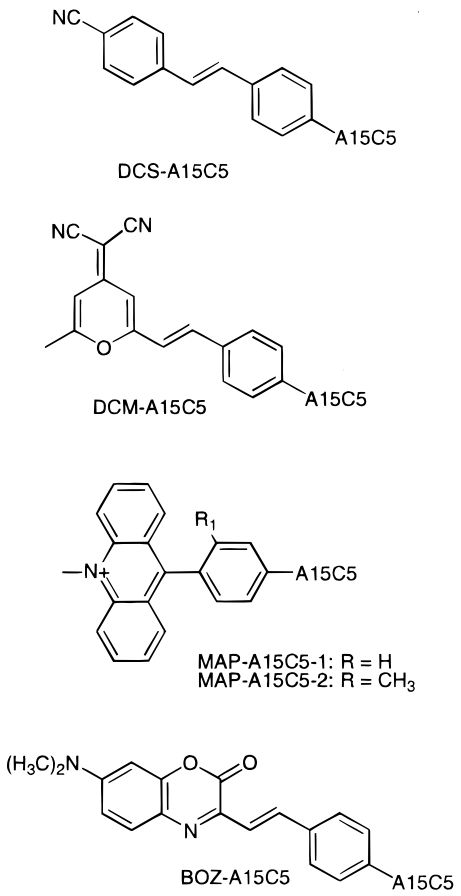

Singular value decomposition analysis of a set of either spectra yielded only a single component with high significance.[73]

A measure for the strength of an ICT process is obtained by analysis of the spectroscopic data as a function of solvent polarity. Since most asymmetric organic dye molecules are characterized by different charge distributions in the ground and first excited singlet state (resulting in different dipole moments), the stabilization of both states involved in the optical transitions is different in a solvent of given polarity. Hence, the dependence of the spectral band position on solvent polarity deviates for absorption (lowest energy band) and fluorescence. Analysis of this solvatochromic behavior allows us to estimate the nature of the absorbing and the emitting species. In the present work, the widely used Lippert−Mataga formalism (eqs 6−8)[72,74] was employed.

$$\Delta\tilde{\nu}(\text{abs} - \text{em}) = \Delta\tilde{\nu}^{\text{vac}}(\text{abs} - \text{em}) + \frac{2(\mu_{\text{es}} - \mu_{\text{gs}})^2}{hc_0a_{\text{o}}^3}(f(\epsilon_{\text{r}}) - f(n)) \quad (6)$$

$$\tilde{\nu}(\text{em}) = \tilde{\nu}^{\text{vac}}(\text{em}) + \frac{2\mu_{\text{es}}(\mu_{\text{es}} - \mu_{\text{gs}})}{hc_0a_{\text{o}}^3}\left(f(\epsilon_{\text{r}}) - \frac{1}{2}f(n)\right) \quad (7)$$

$$f(\epsilon_{\text{r}}) = \frac{\epsilon_{\text{r}} - 1}{2\epsilon_{\text{r}} + 1} \quad \text{and} \quad f(n) = \frac{n^2 - 1}{2n^2 + 1} \quad (8)$$

Here, $\Delta\tilde{\nu}^{\text{vac}}$(abs-em) ($\tilde{\nu}^{\text{vac}}$(em)) is the Stokes shift (emission maximum) in a vacuum, μ_{gs} and μ_{es} are the dipole moments of the ground and the excited state, h is the Planck constant, c_0 is the speed of light in a vacuum, a_{O} is the Onsager cavity radius, and ϵ_{r} and n are the relative permittivity and the refractive index of the corresponding solvent. Graphical analysis of a plot of the Stokes shift (or the emission maximum) vs the solvent polarity function (last terms in eqs 6 and 7) allows the determination of ($\mu_{\text{es}} - \mu_{\text{gs}}$) and μ_{es} (if μ_{gs} is known). For all the D−A-chalcones investigated, good correlations ($r \geq 0.99$) are found (Figure S2) and the differences in dipole moments are determined to be 19.7 D (**1a**), 22.6 D (**1c**), 20.2 D (**1e**), 12.8 D (**2a**), and 18.0 D (**3**).[75] Furthermore, a comparison of the data obtained with eqs 6 and 7 (the Stokes shift involving transitions in both absorption and emission vs the emission band maximum only; Table S3) suggests that, besides possible involvement of other (e.g., highly polar) excited states, the initially formed localized or delocalized excited state is already polar. Correlations of the solvatochromic data (Stokes shift, emission band maximum) with empirical solvent polarity scales ($E_{\text{T}}(N)$, SPP^N)[76] support these findings.[77] A detailed description of the solvatochromic analysis and the correlations with empirical solvent polarity scales is given in the Supporting Information, section S7.

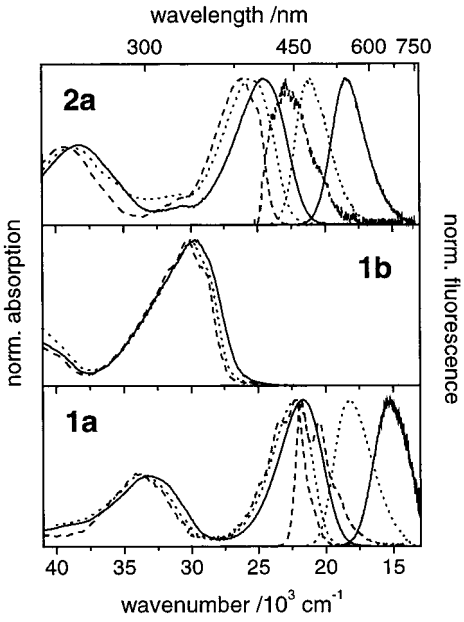

Figure 3. Normalized steady-state absorption and emission spectra of **1a**, **1b**, and **2a** in *n*-hexane (---), diethyl ether (•••), and acetonitrile (—) at 298 K. For the emission band positions of very weakly fluorescent **1b**, see Table S1.

Fluorescence Quantum Yields. The fluorescence quantum yields of the compounds studied largely depend on both the nature of the 4′-substituent and the solvent polarity. In polar aprotic solvents such as acetonitrile, the fluorescence quantum yields of **1a**, **1c**, **1d**, and **1e** with a benzothiazole acceptor are rather low and decrease in the order **1d** ($\phi_{\text{f}} = 0.02$) > **1c** (0.007) > **1a** (0.002) > **1e** (0.001, Table S1). In contrast, phenyl-containing **2a** and **2c** emit moderately with quantum yields of ca. 0.2 in acetonitrile, respectively (Table S2). Here, again, the crowned compound ($\phi_{\text{f}} = 0.25$) is more fluorescent than the DMA compound (0.15) and the julolidino-substituted compound shows the weakest fluorescence (0.015).[79] Similar effects have been observed for other ICT fluorescent probes, their dimethylanilino and julolidino derivatives.[15,65,80] The reduced mobility of the donor group, i.e., its bulkiness, and the different electron-donating properties of the tertiary amine substituents employed account for these results. The bulkiness of the donor substituents

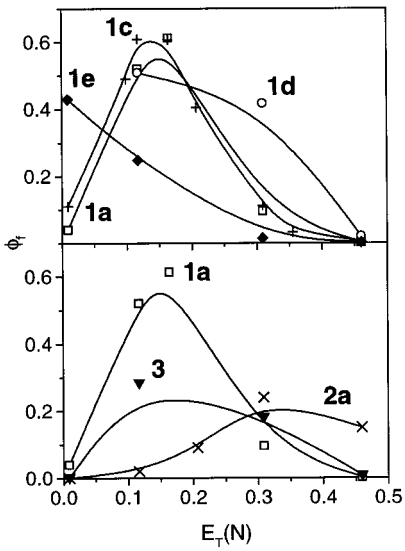

Figure 4. Plots of ϕ_f vs $E_T(N)$ for the D−A-chalcones investigated. Top: **1a** (□), **1c** (+), **1d** (○), **1e** (◆). Bottom: **1a** (□), **2a** (×), **3** (▼). The solid lines are only guides to the eye, and data in protic solvents are omitted (because of low solubility, no data were obtained for **1d** in *n*-hexane).

increases in the order DMA ≪ Jul < A15C5 < $AT_4$15C5[81] and the donor strength of the amino nitrogen decreases in the order Jul > DMA ∼ A15C5 > $AT_4$15C5, as follows from the bathochromic shifts of the corresponding spectra of **1a**, **1c**, **1d**, and **1e** (Figure 2, Table S1).

The lines in Figure 4, although they are only guides to the eye, indicate an opposing behavior of the solvent polarity dependence of the fluorescence quantum yields of **1a**, **1c**, **1d**, **1e**, **2a**, and **3**. A maximum is seen for most compounds in the ϕ_f vs $E_T(N)$ plot and appears in *n*-hexane (no rising edge) for the D−A-chalcone with the strongest ICT character (**1e**) and for that with a considerably weak ICT character (**2a**) between THF and acetonitrile. A reduction in solvent polarity strongly enhances the fluorescence quantum yield of **1a**, **1c**, **1d**, and **1e** but leads to a loss in fluorescence intensity for **2a**. The trends in the two regions can be ascribed to the so-called "negative solvatokinetic behavior", i.e., increasing fluorescence quantum yield with increasing solvent polarity, and the "positive solvatokinetic behavior" where a decrease in emission results from the excited-state population of a highly polar charge transfer state.[82,83] Both possibilities will be discussed below. In alcohols, all the compounds show low fluorescence quantum yields (≤0.011, Tables S1 and S2).

3.3. Time-Resolved Emission of the Dyes at 298 K. *Fluorescence Lifetimes.* Owing to the weak fluorescence of most chalcones, the time-resolved emission data published in the literature until today are very sparse. Generally, their fluorescence lifetimes are referred to as being "within the temporal resolution of the instrument", i.e., (much) shorter than 1 ns.[52] Only recently, Wang and Wu published fluorescence decay times of **2a** and two of its bridged derivatives in various solvents at room temperature and reported single-exponential decay kinetics for all the three compounds studied independent of solvent used, i.e., for instance, 0.70 ns for **2a** in acetonitrile.[56] This lack of time-resolved emission data further encouraged us to study the fluorescence decay kinetics of the D−A-chalcones in more detail. For all the compounds investigated here, monoexponential decay kinetics were only observed in highly polar, aprotic solvents such as acetonitrile or acetone (Figure 5B). In all the other cases, the fluorescence decay profiles could only be fitted to at least two exponentials (Figure 5A,C,D). In medium and apolar solvents, a main decay component is observed and the minor species have either a positive amplitude over the whole emission spectrum (e.g., *n*-hexane) or a negative amplitude at the low-energy side of the emission spectrum (e.g., diethyl ether). In some cases, extrapolation of the ratio of the decay associated spectra ($DAS_i(\lambda)$) of the corresponding decay components (for a detailed description of the formalism, see refs 84 and 85) does not converge at the edges of the spectra, pointing to a more complex behavior than a simple two-state (precursor → successor) reaction scheme with excitation of a single ground-state species, as is, for instance, observed for some D−A-biaryls.[19]

Moreover, for **1a** and **1c**, two decaying species with distinctly different decay times and only slightly changing (with observation wavelength) positive relative amplitudes are found in *n*-hexane.[86] For a comprehensive overview, the lifetimes of the main emitting species are included in Table 2. The behavior in alcohols will be discussed separately below. Furthermore, excitation wavelength-dependent time-resolved studies suggest that either different ground-state species are excited or that CT formation rates depend on the frequency of incident light.[87]

Generally, the data given in Table 2 agree with the solvent dependence of the fluorescence quantum yields, i.e, for example, an increase in lifetime with decreasing solvent polarity for **1a** and **1c**−**e**. Although a determination of the rate constants for radiative and nonradiative deactivation (k_f and k_{nr})[88] is not possible without separating the rate constants by evaluation and analysis of the excited-state reaction model, the parallel trends suggest a more drastic change (decrease) in k_{nr} compared to k_f upon going to apolar solvents for **1a** and related compounds and the vice versa behavior for **2a**.

Solvation Dynamics in Alcohols. Comparing the fluorescence decay profiles recorded for **1c** in isopropanol and acetonitrile (Figure 5A,B) and the fluorescence lifetimes in these solvents (Table 2), the question of the origin of the nonexponential decay behavior in alcoholic solvents arises. Besides an excited-state reaction involving population of (several) transient species, relaxation of the solvent molecules of the inner and outer solvation sphere ((strong or weak) dipolar interaction with the solute or in the bulk) has to be considered. Moreover, in the case of an excited ICT molecule with a large excited-state dipole moment and a carbonyl group in the acceptor part, in polar solvents capable of hydrogen bond formation (such as alcohols), solute−solvent interactions can occur, leading to exciplex formation (with the precursor complexes possibly being already present in the ground state), which are more or less nonfluorescent.

When a strong dipole, e.g., the excited dye molecule, interacts with the inner solvation sphere, those solvent molecules loose their (dipolar and long range) orientational correlations and relax in an individual manner. On the other hand, solvent molecules in the bulk (outer solvation shell) maintain their properties and relax in a collective way. Whereas the latter process is comparatively fast and can be quantified by the solvent longitudinal relaxation time τ_l, the former process can be much slower depending on the degree or strength of direct interaction between the solvent molecule and the solute and is referred to as the microscopic reorientation time or (average) solvation time (τ_M, $\langle\tau\rangle$).[78,89−93] For weakly interacting solvents such as acetonitrile or acetone, τ_l and $\langle\tau\rangle$ are rather similar and on the order of a few hundered femtoseconds,[90] but for alcohols at room temperature both times are on the order of a few picoseconds.[90−92] Especially for alcohols, which are "aggregated solvents" capable of strong hydrogen bond formation, the temporal relaxation

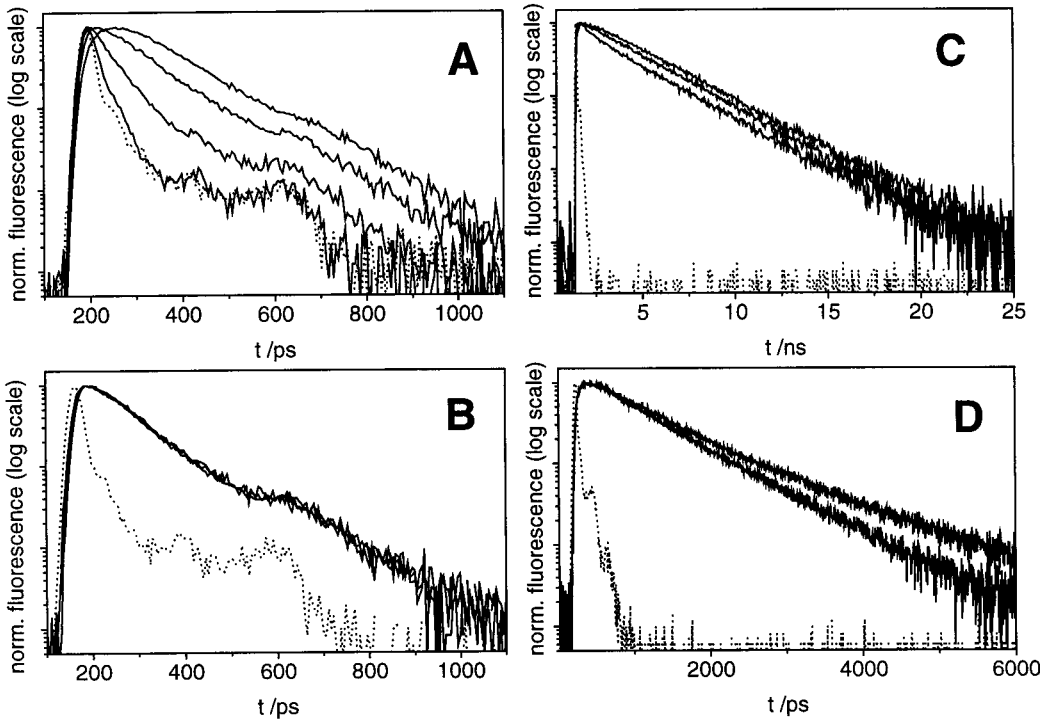

Figure 5. Fluorescence decay curves of **1c** in different solvents at 298 K. (A) Isopropanol, excitation at 456 nm, emission at 710, 605, 560, and 500 nm (from top to bottom). (B) Acetonitrile, excitation at 456 nm, emission at 720, 640, and 560 nm. (C) Diethyl ether, excitation at 428 nm, emission at 640, 560, and 500 nm (from top to bottom). (D) *n*-Hexane, excitation at 428 nm, emission at 560 and 480 nm (from top to bottom). Dotted curve = IRF.

TABLE 2: Main Decay Species of 1a, 1c, 1d, 2a, and 3 in Selected Solvents at 298 K

	solvent	τ_f ps		solvent	τ_f ps
1a	EtOH	10, 22 (19)[a]	**1d**	EtOH	11, 22, 64 (14)[a]
	MeCN	25		MeCN	170
	Et_2O	950, 3090		CH_2Cl_2	2240
	Hex	180, 690[b]		Et_2O	1060, 2790
1c	MeOH	7, 14 (17)[a]	**2a**	EtOH	9, 33, 41 (20)[a]
	EtOH	19, 35 (24)[a]		MeCN	870
	PrOH	13, 46, 91 (27)[a]		CH_2Cl_2	1120
	EG	11, 45 (17)[a]		Et_2O	150, 550[c]
	MeCN	74	**3**	EtOH	23, 31 (12)[a]
	Acetone	270		MeCN	100
	CH_2Cl_2	850		CH_2Cl_2	1550
	THF	2230		Et_2O	750, 2080
	Et_2O	780, 3090		Hex	11

[a] Apparent decay times were obtained by simultaneously fitting N (in brackets) decays to i linked lifetimes (the program varies only the preexponential factors). Although global analysis is not the adequate model to describe the relaxation behavior, this fitting routine was used in order to obtain comparable quantities, i.e., apparent lifetimes (in all the cases *global* $\chi_R^2 < 1.3$). [b] $a_{rel}^1(\lambda) = a^1(\lambda)/\Sigma a^i(\lambda) = +0.4$ to $+0.6$. [c] 290 K.

phenomena largely depend on the location of the single solvent molecule with respect to the solute.

For fluorescent molecules with $\tau_f \gg \tau_l$, the measurement of the time-dependent fluorescence (Stokes) shift or the determination of the spectral response function of the dye molecules in a certain solvent yields the characteristic solvation times within relatively good agreement.[90,92,94] However, for molecules where an excited-state reaction involving two or three species occurs, the rate constants are predominantly dependent on the molecular structure of the dye itself and often lead to largely different fluorescence decay times (and thus largely different time-dependent spectral shifts) for the related molecules.[84] In this case, analysis of the time-resolved emission spectra (TRES) can give access to the mechanisms probably involved in excited-state deactivation.

The spectral evolution of TRES was determined for **1d** in ethanol and **1c** in isopropanol by monitoring the spectral response function $C_\nu(t)$ (eq 9) of the time-dependent solvation process.

$$C_\nu(t) = \frac{\nu(t) - \nu(\infty)}{\nu(0) - \nu(\infty)} \tag{9}$$

Here $\nu(t)$, $\nu(0)$, and $\nu(\infty)$ are the characteristic frequencies at the corresponding observation time.[96] As an example, TRES and a plot of $C_\nu(t)$ of **1d** in ethanol are given in Figure 6.

Comparison of the fitting results of the correlation function $C_\nu(t)$ (τ_1, τ_2 indicated in Figure 6, $\langle\tau\rangle = 19$ ps) shows that the data obtained in ethanol are comparable to the times found by Horng et al. in the same solvent at 295 K for the spectral response function of a coumarin dye, i.e., slow components τ_i of 5.03 and 29.6 ps and $\langle\tau\rangle = 16$ ps.[90] Room-temperature data on isopropanol are sparse but a comparison of low-temperature data on *n*-propanol and isopropanol and extrapolation of the data for the latter suggests, that the τ_i of 13 and 54 ps ($\langle\tau\rangle = 35$ ps) found here for **1c** (Figure S3) are of the same order of magnitude.[90,92] However, as in the case of the fluorescence lifetimes given in Table 2, the values obtained here for $\langle\tau\rangle$ are apparent values and do not reflect the real solvent relaxation times.

Apparently, for the D−A-chalcones, the fluorescence decay times in alcohols are of similar magnitude as the relaxation times of the protic solvents itself (e.g., $\tau_l = 16$ ps, $\tau_M = 47$ ps for ethanol[93] and data in Table 2).[89,90,92] Moreover, hydrogen bond formation at an acceptor carbonyl group (found for coumarins, which are very similar in this respect to D−A-chalcones) was found to be operative on the same time scale as well (e.g., ca. 15 ps in methanol).[95] On the other hand, the differences in

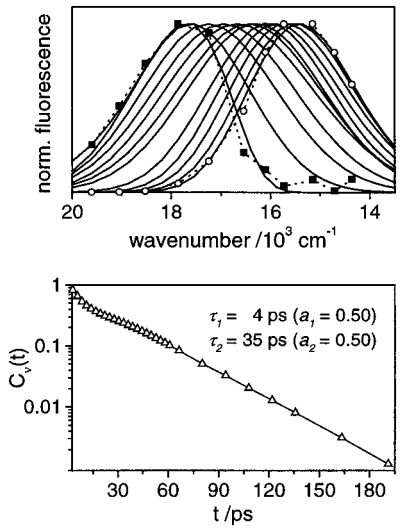

Figure 6. Upper part: spectral reconstruction of the wavelength-resolved fluorescence decay of **1d** in ethanol at 298 K. Solid lines correspond to log-normal fits and dotted lines to the actual data points converted to the frequency scale (squares at $t = 0$, circles at $t = \infty$). Lower part: fit of the spectral response function $C_v(t)$ to two exponentials indicated in the plot.

fluorescence lifetime data for **1a** and **1d** in alcohols (e.g., τ_f(**1d**) $\sim 3 \times \tau_f$(**1a**) for the slow components, Table 2) are evident but less pronounced compared to those in a "fast" relaxing solvent such as acetonitrile, where only the excited-state relaxation is monitored (Here, solvent relaxation is >100 times faster than fluorescence, τ_l(MeCN) = 0.2 ps,[97] and τ_f(**1d**) $\sim 7 \times \tau_f$(**1a**), Table 2.). The monoexponential decay kinetics in acetonitrile suggest that in these polar aprotic solvents only a single emitting species is present, pointing to a straightforward excited-state reaction mechanism (e.g., fast population of a single highly polar emissive state, see below).

As a consequence, the prerequisites accounting for the large differences in acetonitrile (a factor of 7 between the DMA and $AT_4$15C5 derivative) are still present in alcohols but obscured by another effect. This is further confirmed when comparing the lifetimes of **2a** in both solvents (870 ps in acetonitrile and a long-lived component of 41 ps in ethanol). Most probably the crucial effect is hydrogen bond formation.

Thus, for the D−A-chalcones in alcohols, solvent relaxation, hydrogen bond formation, and deactivation of the emitting singlet state cannot be monitored or analyzed separately. Accordingly, the fluorescence decay times given in Table 2 are only apparent τ_f describing the superimposed processes, and global analysis of the wavelength-resolved fluorescence decay data according to an excited-state reaction mechanism involving discrete species is misleading in this case.

3.4. Temperature-Dependent Behavior. Investigation of the temperature-dependent absorption and (steady-state as well as time-resolved) emission behavior of **1a**, **1c**, **1d**, **1e**, and **2a** in ethanol and of **1a** and **2a** in diethyl ether generally supports the results of the studies at 298 K: (i) **1a**, **1c**, and **1d** show very similar tendencies in ethanol (increase in fluorescence quantum yield, line-narrowing of the bands, Figure S4, Table S5), (ii) **1a** and **2a** show pronounced differences in cooled diethyl ether solution (drastic decrease in k_{nr} only for **2a**) but behave the same in the glass where all rotational motions are frozen (Figure S5, Table S5), and (iii) the dynamic emission behavior is conserved above the glass point in both diethyl ether and ethanol; i.e., even in an alcohol solution at low temperature, solvent dynamics intermingle with fluorescence deactivation, thus obscuring a straightforward analysis of an excited-state reaction mechanism that involves molecular motions and different excited states (a description of the temperature-dependent behavior is provided in the Supporting Information, section S8.).

3.5. Spectroscopic Behavior of 1b. For the model compound **1b**, containing only the phenyl ring as a considerably weak donor, the solvent-dependent shifts in absorption and emission are much less pronounced (Figure 3, Table S1). A similar behavior has been previously described for other chalcones carrying weak donors in position 4′ (and cf. **1f** in Table S1).[49,54] **1b** shows both a strongly blue-shifted absorption and emission band compared to its amino donor-substituted derivatives and has the lowest fluorescence quantum yield of the chalcone series in all the solvents investigated. Additionally, its main absorption band centered at ca. 29 700 cm^{-1} has an asymmetrical shape in all the solvents employed and resembles a linear combination of a stronger absorption band at ca. 31 800 cm^{-1} and a weaker band at ca. 29 100 cm^{-1}, respectively. Both subbands show the similar slight dependence on solvent polarity. Concerning the origin of these bands, the absorption band of **6** (the acceptor composite: $\tilde{\nu}$(abs) = 34 010 cm^{-1}, $\epsilon[\tilde{\nu}(\text{abs})]$ = 11 700 M^{-1} cm^{-1} in acetonitrile; $\tilde{\nu}$(abs) = 34 250 cm^{-1}, $\epsilon[\tilde{\nu}(\text{abs})]$ = 12 100 M^{-1} cm^{-1} in diethyl ether) is found in a different wavelength region and a transition localized on the 4-substituted cinnamoyl fragment of the chromophore should appear in the same wavelength region. Thus, in accordance with results obtained by Szmant and Basso in a study of derivatives carrying a Ph−CO-acceptor group,[47] no hints for such localized transitions were found. This is further supported by the mismatch of the absorption and luminescence excitation spectrum, i.e., the excitation spectrum being shifted to lower energies (ca. 27 700 cm^{-1}; note that **6** was found to be nonfluorescent).

3.6. Photophysical Mechanisms. Recently, we have shown for a series of bridged derivatives of **2a** that the population of several highly polar excited states seems to be involved in the deactivation of the D−A-chalcone's S_1 state.[79] Moreover, different conformers are possibly present already in the ground state and can further complicate a photophysical reaction scheme.[50,79] As depicted in Scheme 3, for **1a**−**f** not only s-cis ("*c*") and s-trans ("*t*") single bond isomerism (as for **2a**−**c**) is possible but also a further syn and anti isomerism concerning the benzothiazole nitrogen and the carbonyl oxygen atom can occur (to avoid "cis" and "trans" as well as "double bond" and "s-isomer" misunderstandings, the double bond isomers are labeled *E* and *Z* and the single bond isomers *c* and *t*, arriving at *cE*, *tE*, *cZ*, and *tZ conformers*, as depicted in Scheme 3).[98] In analogy to the results reported for **2a**,[79] the occurrence of energetically and electronically similar rotamers is also found for **1a**, **1d**, **1e**, and **3** in quantum chemical calculations (Table S6). Such phenomena are well-known, for instance, for naphthyl-phenyl-substituted ethylenes[99] and for related benzoxazinone styryl derivatives.[80] Furthermore, X-ray as well as IR studies of numerous chalcones showed that either *cE* or *tE* conformers are preferred in certain molecules in the crystalline state[100,101] or that both conformers can be present in solution.[102] As has been already mentioned above, both **1c** and **1d** crystallize in the *anti-cE* conformation (Figure 1 and Scheme 3). For **2c**, the same features apply as described for **2a** and its bridged derivatives[79] and here, only the main implications for the benzothiazole derivatives **1a** and **1c**−**e** are discussed.

For **2a** and **2c**, showing a negative solvatokinetic behavior (Figure 4), the adiabatic photochemical reaction mechanism involved includes a fluorescent all-planar excited conformation

SCHEME 3: Chemical Structures of Possible Chalcone Conformers[a]

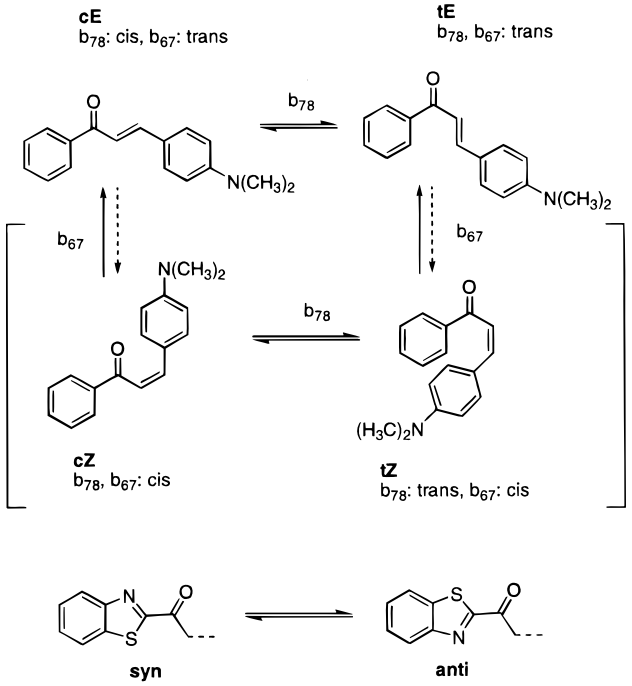

[a] The bonds affected by a 180° twist are labeled according to a formula in Scheme 1A. In the top row, the two stable conformers of the double bond b_{67} *E* isomer and in the middle row, the sterically unfavorable *Z* conformers are shown. The conformation of bonds b_{67} and b_{78} is indicated and the labels on the arrows denote the bonds which have to rotate for the respective transition. In the bottom row, the syn/anti isomerism of the benzothiazole-substituted derivatives is shown.

E*, a nonfluorescent C=C twisted species with biradicaloid properties and reduced dipole moment (P* state) and (at least) two C−C twisted species of highly polar nature, fluorescent (A* state, twist of anilino bond b_{56}, Scheme 1) as well as nonfluorescent (K* state, twist of bond neighboring the carbonyl group), A* and K* being related to the TICT mechanism.[79,103] Moreover, in apolar solvents such as *n*-hexane, besides formation of a weakly polar P* state, the emitting state(s) is (are) sufficiently destabilized to experience perturbation by the proximity effect, i.e., vibronic coupling of energetically close lying nπ* states.[104] Population of an emissive triplet state was found to be of no great significance for these D−A-chalcones,[79] which is supported by observations published so far by other research groups.[51,55]

A close spectroscopic relation of both conformers has been found exemplified by spectrally similar absorption and emission characteristics of derivatives fixed in the *cE* (b_{78}- and b_{89}-bridged analogue of **2a**)[52,57,79] or *tE* conformation (all-bridged derivative of **2a**).[57] In the case of the unbridged compounds being able to adopt both a *cE* and/or *tE* conformation, e.g., **2a** (or **1a**−**f**, **2c**, and **3**), the ground-state equilibrium between both conformers is largely dependent on the solvent stabilization of each conformer. However, no direct evidence for simultaneous excitation of conformers could be yet detected.[79]

The studies reported here reveal a (partly) positive and/or (partly) negative solvatokinetic behavior for **1a**, **1c**−**e**, and **3**. With the exception of **1e**, for these compounds the fluorescence is considerably lower in *n*-hexane compared to diethyl ether (Figure 4 and Table S1). Only for **1e** does the increase in fluorescence quantum yield in this polarity region suggest that the emissive state is still of considerably lower energy and both interaction by the proximity effect and population of a non-

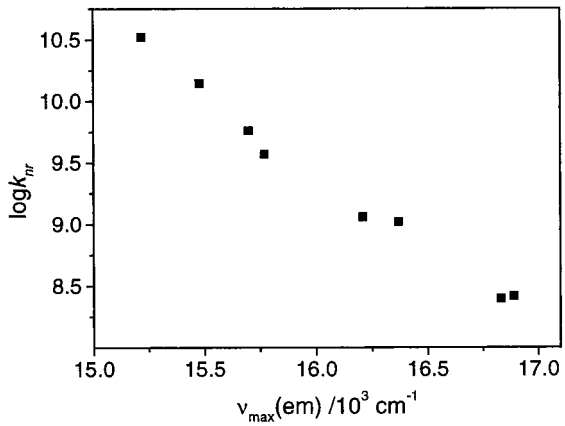

Figure 7. Plot of log k_{nr} vs $\tilde{\nu}$(em) for **1a**, **1c**, and **1d** in solvents of polarity between acetonitrile and THF.

emissive P* state are suppressed in *n*-hexane to a major extent. Thus, the fact that the maximum of a ϕ_f vs $E_T(N)$ plot is shifted to less polar solvents with increasing charge-transfer character fits well into the picture derived from the (bridged) phenyl derivatives.[79]

The temperature dependence of the fluorescence quantum yields and lifetimes of **1a** and **2a** in diethyl ether (see sections 3.4 and S8) gives further evidence in favor of this explanation. Whereas **2a** shows a behavior known for compounds displaying reduced emission due to P*-state formation,[105] i.e., a strong increase in fluorescence quantum yield upon freezing of the radiationless relaxation channel P* (ϕ_f = 0.02 at 290 K and 0.74 at 170 K), this tendency is absent in **1a** being already highly fluorescent at room temperature (ϕ_f = 0.52). Furthermore, a comparison of the solvatochromic behavior of **1a** and **1e** suggests that the stronger ICT in the latter compound leads to red-shifted spectra and lower fluorescence quantum yields owing to the energy gap law.[106] The linear correlation obtained when plotting log k_{nr} of **1a** and the crowned derivatives as a function of emission energy (for solvents of polarity between acetonitrile and THF) points to a dependence of nonradiative deactivation on donor strength according to the CT character and the energy gap rule (Figure 7). Assuming that no other process contributes to excited-state depopulation, a decrease in energy gap between the emissive and corresponding ground state leads to an increased probability for internal conversion (ic) and only k_{ic} is accelerated. The absence of any major influence of a rotation around the amino bond is stressed by the small differences between bulky **1c** and **1a**. Similar observations for dimethylamino and julolidino derivatives of D−A-dyes have been made by Wang, Fery-Forgues et al., and us.[52,79,80] However, different probabilities for A*- and K*-state formation in excited **1a** and **1e** can also play a role.

In H-acidic solvents, i.e., alcohols, the fluorescence of all the compounds investigated here is weak and solvent relaxation intermingles with excited-state deactivation; i.e., all the processes occur on a similar time scale. Whereas the emission of **1a**, **1c**−**e**, and **3** is already weak in acetonitrile, the fluorescence of **2a** and **2c** is quenched (factor of 15 for **2a**) when going from acetonitrile to ethanol (Table S2). Hydrogen-bonding interactions preferably occurring at the carbonyl group of the acceptor and solute−solvent complexes being possibly (already) present in the ground state account for the enhanced nonradiative losses and quenching of A* fluorescence in the case of the phenyl derivatives.[52] Accordingly, any H-bond interaction (with the acceptor fragment of the molecule) should increase in size upon a charge-transfer process taking place after excitation.[107]

TABLE 3: Spectroscopic Properties of the Cation Complexes of 1d in Acetonitrile[a]

	$\tilde{\nu}$(abs), 10^3 cm^{-1}	$\tilde{\nu}$(em), 10^3 cm^{-1}	$\Delta\tilde{\nu}_{cp-fp}$(abs), cm^{-1}	$\Delta\tilde{\nu}_{cp-fp}$(em), cm^{-1}	ϕ_f	τ_2, ps	τ_3, ns	log K_S(abs)	r_M,[b] Å	$\chi_m^2 r_M$[c]
1d[d]	21.98	15.70			0.02	170				
⊂**Hg**^{II}	29.30	17.00	7320	1300	0.12	568	1.07	>5.5 [e]	1.02	4.08
⊂**Zn**^{II}[f]									0.74	2.01
⊂**Cu**^{II}	30.11[g]	18.15[h]	8130	2450	(0.009)[h]	202	1.15	n.d.	0.73	2.64
⊂**Cu**^{I}									0.96 (4)	3.46
⊂**Ag**^{I}	22.88	16.49	900	790	0.05	348		4.51	1.15	4.28

[a] The experiments were carried out up to the micromolar concentration range for heavy and transition metal ions and up to the millimolar concentration range for alkali and alkaline-earth metal ions[164] ($c_L = 3 \times 10^{-6}$ M; the short decay components τ_1 are not included; for discussion, see text; cp = complexed probe, fp = free probe, n.d. = not determined). [b] All the radii were taken from ref 120 and are for six-coordination except where the coordination number is indicated in brackets[165] and for Cu^{I}.[166] For Cu^{I}, tetrahedral coordination is found in most polythia ether complexes.[148,149] [c] The electronegativity values given in the literature differ largely in units.[167] Here, the softness or class B parameter[118] was calculated with the electronegativity values of Allred and Rochow.[168] [d] No effects observed for Li^{I}, Na^{I}, K^{I}, Mg^{II}, Ca^{II}, Sr^{II}, Ba^{II}, and Pb^{II}. [e] Too high to be determined with acceptable accuracy with the method employed. [f] A similar behavior is observed for Cd^{II} ($r_M = 0.95$, $\chi_m^2 r_M = 2.71$), Ni^{II} (0.69, 2.52), and Co^{II} (0.74, 2.61). [g] For **1d**⊂Cu^{II}, various subbands, exemplified by shoulders in the absorption spectrum (e.g., at 36 000 and 23 000 cm^{-1}) were found, their origin being unclear at present (see text). [h] For **1d**⊂Cu^{II}, a second emission band at 23 200 cm^{-1} is observed whose origin is still unclear (see text).

In the case of **1b**, no noticeable CT interactions are operative and the initially excited state undergoes very fast nonradiative deactivation, which may be either ascribed to the "proximity effect", i.e., vibronic coupling of energetically close lying nπ* and $\pi\pi$* states, or efficient P*-state formation (with or without consecutive triplet population, see above).[51] Assuming an analogy to stilbenes, excitation of **1b** should lead to the formation of weakly polar E* but the corresponding P* state should be of higher polarity.[83] Accordingly, the energy level position of P* should be more strongly stabilized by polar solvents, leading to enhanced quenching in these solvents. However, from the generally low fluorescence quantum yields of **1b** ($\phi_f < 2 \times 10^{-4}$) no such trend can be derived (Table S1). A comparison with **1f**, spectrally displaying CT characteristics but still being weakly fluorescent in solvents of any polarity ($\phi_f < 2 \times 10^{-4}$, Table S1), indicates that most probably efficient P*-state formation is operative in both molecules regardless of the substitution pattern. Since all the other D−A-chalcones lacking an amino donor described in the literature so far are only weakly fluorescent at best,[108] the formation of a fluorescent A* state can be excluded for these molecules. For **2b** which was found to be nonfluorescent, a similar mechanism should be expected. This is supported by findings of other research groups.[50,51]

3.7. Absorption and Fluorescence Behavior of the Complexes. As discussed above, the spectroscopic behavior of **1a**, **1c**−**e**, **2a**, and **2c** is relatively straightforward in acetonitrile. In this highly polar aprotic solvent where the complexation studies were carried out, the polar emissive A* and nonemissive K* state are rapidly populated, resulting in largely Stokes-shifted, broad (NIR) emission bands and monoexponential decay kinetics.

*Complexation Behavior of **1d**.* The fluorescent probe carrying the monoaza tetrathia macrocycle AT$_4$15C5 is expected to strongly coordinate "soft" heavy and transition metal ions, especially the thiophilic ions Ag^{I}, Cu^{I}, and Hg^{II} whereas binding of "hard" main group metal ions should barely occur. With the exception of Cu^{I} (see below), this is confirmed by a comparison of the data given in Table 3 and the spectra shown in Figure 8.

As follows from both Figure 8 and Table 3, the hypsochromic shifts observed in absorption are rather large compared to those in emission. Moreover, these shifts are much more pronounced for the divalent metal ion Hg^{II} (7320 cm^{-1} in absorption, 1300 cm^{-1} in emission) as compared to monovalent Ag^{I} (900 cm^{-1} in absorption, 790 cm^{-1} in emission). The isosbestic points observed in both cases in a UV/vis-spectrophotometric titration experiment indicate the formation of a single equilibrium, i.e.,

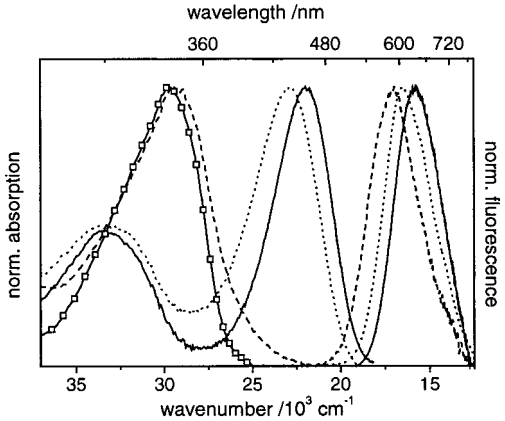

Figure 8. Normalized steady-state absorption and emission spectra of **1d** (—) and its Ag^{I} (•••) and Hg^{II} (---) complexes in acetonitrile. The absorption spectrum of **1b** (□) is included for comparison.

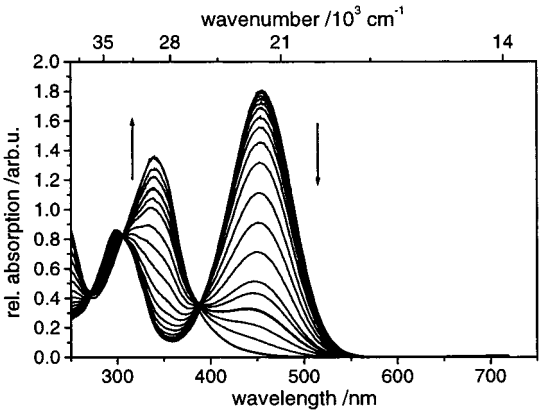

Figure 9. UV/vis-spectrophotometric titration spectra of **1d** with Hg^{II} perchlorate in acetonitrile ($c_L = 9 \times 10^{-6}$ M, Hg^{II} addition in the range of $0.008 \le x_{M/L} \le 20$; $x_{M/L}$ = metal ion-to-ligand ratio). For a better comparison, similar scales were chosen for the *x*-axes of Figures 9 and 15.

1:1 complexes (Figure 9). The total abstraction of the nitrogen lone electron pair from the chromophore π-system in the case of Hg^{II} (cf. absorption spectra of **1d**⊂Hg^{II} and **1b** in Figure 8) indicates strong electrostatic interaction between the ion bound in the cavity of the receptor and its nitrogen donor atom. This is generally supported by the X-ray structure of *N*-phenyl-AT$_4$-15C5⊂Ag^{I} (section 3.1), where the hybridization of the crown ether nitrogen atom was found to change from sp^2 in the free probe to sp^3 in the complex. Furthermore, the high selectivity of this receptor for thiophilic metal ions such as Ag^{I} and Hg^{II}

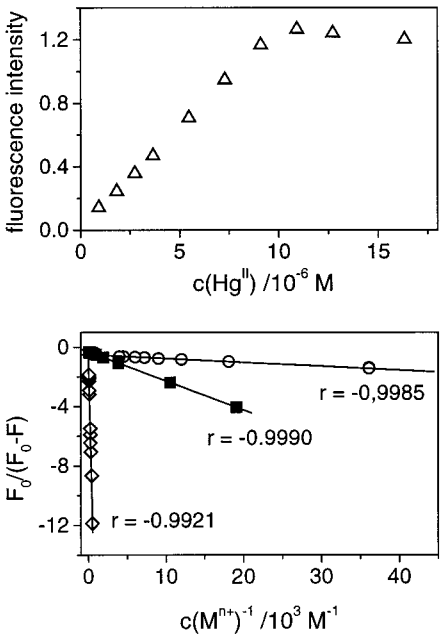

Figure 10. Fluorometric titration of **1d** with Hg^{II} (top) and Ag^{I} (○, bottom) and of **1c** (bottom) with Na^{I} (◇) and Ca^{II} (■) perchlorates in acetonitrile ($c_L = 9 \times 10^{-6}$ M (**1d**), 1×10^{-5} M (**1c**), excitation at the isosbestic point, data of Ag^{I}, Na^{I}, and Ca^{II} titration fitted to eq 4).

is demonstrated by the lack of spectroscopic changes upon addition of Zn^{II}, Cd^{II}, Ni^{II}, or Pb^{II} salts (Table 3).

Even more interestingly, for **1d**, not only in the case of Ag^{I} but also for the known fluorescence quencher Hg^{II} (heavy atom effect),[39] a complexation-induced fluorescence enhancement occurs. Moreover, in the case of Hg^{II}, the observed fluorescence enhancement factor FEF of 6 is considerably high for an ICT fluorescent probe.[109] Of all the metal ions employed in these studies, only Cu^{II} was found to interfere with the determination of Hg^{II} and Ag^{I}; i.e., complexation-induced changes occur also in the presence of Cu^{II} (see below). The formation of well-defined complexes[110] is reflected by a simple relationship between the fluorescence (or absorption) signal and metal ion concentration and leads to linear calibration graphs (Figure 10).

Time-resolved fluorescence measurements performed with **1d** and Ag^{I} as well as Hg^{II} show that in accordance with the observed increase in fluorescence quantum yield, cation complexation of the probe is also accompanied by the appearance of a new (Ag^{I}) or two new (Hg^{II}) long-lived decay component(s) with cation specific fluorescence lifetimes between 350 ps and 1 ns (Table 3). Under conditions where complex formation is complete, biexponential decay kinetics are noticed for Ag^{I} and the kinetics of the Hg^{II} complex involve (at least) three decay components. For Hg^{II}, both long-lived decay components show a positive amplitude over the whole range of the emission spectrum and largely overlapping spectra.

When the wavelength-resolved fluorescence decay data of the complexes is analyzed at full complexation, at the far blue edge of the emission spectrum a fast decay component (τ_1) of 55 ps (for Ag^{I}) and 90 ps (Hg^{II}) with a positive amplitude occurs. In the middle and red region of the fluorescence band this component is found as a rise time (negative amplitude). For a better illustration, two decays of **1d**⊂Hg^{II} are shown in Figure 11. For **1d**⊂Hg^{II}, when recording time-resolved emission spectra (TRES) as a function of excitation wavelength (within the excitation range of the second (370−420 nm) and third (310−330 nm) harmonic of the experimental setup employed), two additional lifetimes with positive amplitudes over the whole

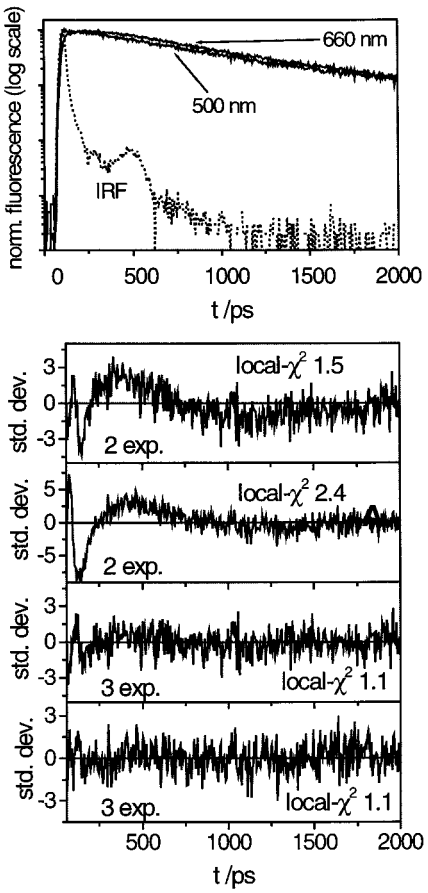

Figure 11. Upper graph: fluorescence decay curves of **1d**⊂Hg^{II} in acetonitrile. Excitation at 380 nm, emission at 500 ($DAS_2/DAS_3 = 0.8$) and 660 nm ($DAS_2/DAS_3 = 1.2$).[116] Lower graph: residuals of the results of the fits. From top to bottom: decays at 500 and 660 nm fitted to two exponentials and the same decays fitted to three exponentials (lifetimes given in the text, *local* χ_R^2 indicated, IRF = instrumental response function).

emission region are found. Globally analyzing a set of 20 decay curves, 10 recorded for each excitation wavelength (380 and 410 nm), always yields three components with lifetimes of 90 ps, 568 ps, and 1.1 ns, respectively (*global* $\chi_R^2 = 1.1$; for two components, *global* $\chi_R^2 = 1.9$).[111] Thus, with both excitation wavelengths employed, only the complex(es) is (are) excited.

Whereas in the case of Cu^{II}, the spectroscopic changes are more complex and involve the appearance of various subbands (of weak intensity) in the absorption spectrum and two fluorescence emission bands, no measurable effects were observed upon addition of Cu^{I} (up to the micromolar concentration range). Since the latter ion shows a high preference for sulfur over nitrogen and prefers a tetrahedral coordination sphere, binding to the receptor, i.e., to its sulfur atoms, could still occur but may escape optical detection (for a detailed discussion, see sections 3.9 and 3.10).[13] The aminophilic Cu^{II} induces fluorescence quenching and the complex shows a nonexponential fluorescence decay behavior, the single decay components depending on both excitation and observation wavelength. Because of its weak fluorescence and the gap in the available excitation range of the laser setup (330−370 nm), the spectroscopic behavior of this complex was not further studied. Explanations for the nature of the Cu^{II} complex will be given in section 3.10 dealing with a second coordination site in the D−A-chalcones.

*Complexation Behavior of **1c**.* Addition of alkali and alkaline-earth metal ions to an acetonitrile solution of **1c** affects both its

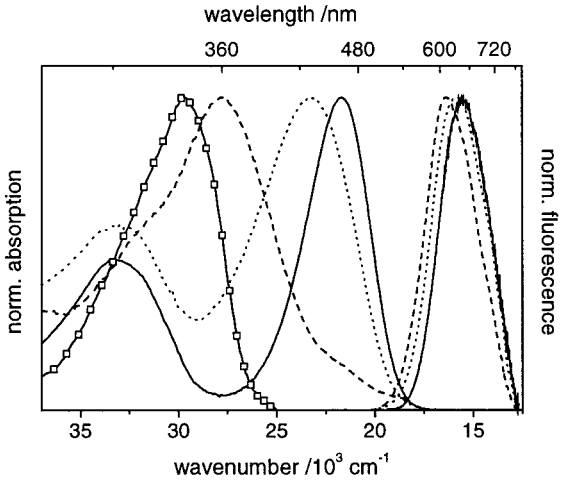

Figure 12. Normalized steady-state absorption and emission spectra of **1c** (—) and its Na^{I} (•••) and Ca^{II} (---) complexes in acetonitrile. The absorption spectrum of **1b** (□) is included for comparison.[162]

absorption and emission behavior. Similar to the cation-induced spectroscopic effects described for **1d** and various thiophilic ions, binding of **1c** to the monovalent cations Li^{I}, Na^{I}, and K^{I} leads to a small hypsochromic shift in absorption accompanied by a decrease in molar absorptivity. For divalent cations, the hypsochromic shift is much more pronounced (Figure 12) and leads to the appearance of a strongly blue-shifted absorption band of the cation complex located at 28 680 cm^{-1} for Mg^{II}, 27 890 cm^{-1} for Ca^{II}, 27 250 cm^{-1} for Sr^{II}, and 26 320 cm^{-1} for Ba^{II} (Table 4). This effect is indicative for pronounced removal of the lone electron pair of the nitrogen atom of the receptor from the conjugated π-system, as can be derived from a comparison of the absorption bands of **1b** and **1c**⊂Ca^{II} in Figure 12. As for **1d**⊂Ag^{I}, the results of the X-ray analysis of a complex of *N*-phenyl-A15C5 and Ca^{II} further support these findings. The hybridization of the A15C5 crown ether nitrogen atom also changes from sp^2 in the free probe to sp^3 in the complex. Except for Mg^{II}, isosbestic points are observed in all the cases studied, indicating a single equilibrium, and thus, the formation of well-defined 1:1 complexes. For Mg^{II}, in addition to the blue-shifted absorption band located at 28 680 cm^{-1}, the appearance of an additional red-shifted absorption band with a maximum at 17 300 cm^{-1} is noticed.[112] Similar effects as described for Mg^{II} are observed in the presence of Pb^{II}, Hg^{II}, and Cu^{II} at a metal-to-ligand ratio $x_{M/L} > 5$ (i.e., in the micromolar concentration range) suggesting the formation of a second complex of different nature. The special complexation behavior of Mg^{II} along with the complexation reaction occurring with some of the heavy and transition metal ions will be discussed below. Chelation to alkali and alkaline-earth metal ions is further accompanied by a blue shift of the emission band of **1c** and an increase in fluorescence quantum yield by a factor of 4−8.5 depending on the cation bound (Table 4).

The size of both effects is clearly affected by the charge of the cation bound, the strongest hypsochromic shift of 1330 cm^{-1} occurring for Mg^{II} and the highest increase by a factor of 8.5 occurring for Ca^{II}. Furthermore, in the case of Mg^{II}, excitation at the long wavelength absorption band does not yield any measurable fluorescence (this is also observed for the other ions forming this complex; see Table 4). The well-defined 1:1 complexation, important for straightforward analytical applicability, is shown for Na^{I} and Ca^{II} perchlorates in acetonitrile in Figure 10.

Time-resolved fluorescence measurements performed with some alkali and alkaline-earth metal ion complexes of **1c** show that in accordance with the observed increase in fluorescence quantum yield, cation complexation of **1c** is also accompanied by the appearance of a new long-lived decay component with a cation specific fluorescence lifetime of 90−200 ps, which exceeds that of the uncomplexed fluorescent probe by a factor of 1.2−3. Again, under conditions where complex formation is complete, a behavior similar to that of **1d**⊂Ag^{I} is observed for the divalent ions; i.e., a second fast decay component is found. For the monovalent ions, this species could not be detected with a reasonable confidence owing to the temporal resolution of the instrument. The fast decay component detected for Ca^{II} amounts to 50 ps, respectively. In the low-energy region of the spectrum, negative amplitudes are found for these species.

*Complexation Behavior of **2c**.* Binding of alkali and alkaline-earth metal ions by **2c** results in very similar spectral effects, as have been observed for **1c**. But in contrast to **1c** (and **1d**) the complexes display a quenched fluorescence compared to the free probe, a characteristic unfavorable for an analytical application. Thus, a detailed description is omitted here and the main features are only discussed in a following section (section 3.10, Table 5) dealing with the possible coordination sites in the D−A-chalcones.

3.8. Excited-State Deactivation. Cation complexation in the donor part of ICT chromo- and fluoroionophores generally leads to a reduction in the chromophoric π-system resulting in hypso- and hypochromic shifts. This behavior can be rationalized in the general framework of triad theory[113] and the theory on linear conjugated systems[114] as the step from a more asymmetric polymethinic character to a more asymmetric polyenic character. The much less pronounced complexation-induced shifts in emission point to a weakening of the cation nitrogen coordinative bond in the excited state due to electrostatic repulsion.[9−12]

Cation Repulsion in the Excited State. The large Stokes shift of the cation complexes, especially for divalent ions (e.g., 11510 cm^{-1} for **1c**⊂Ca^{II}, Table 4), suggests that absorbing and emitting species are different. In combination with the fast ICT process in these probes, this behavior indicates that electrostatic repulsion between the cation and crown nitrogen atom occurs on the subpicosecond time scale parallel to the CT. Thus, the (red-shifted) emission spectra measured for the complexes do not correspond to the initially excited complex with strong ion probe interaction (LM)* but to its successor (in terms of an excited-state reaction), a relaxed species with weakened cation−donor interaction. This is consistent with the time-resolved emission data, where a fast component is found as a decaying species in the high-energy part of the spectrum and as a rising species (rise time, negative amplitude) in the low-energy part. The lifetime of this species is relatively short, i.e., for instance, 50 ps for **1c**⊂Ca^{II} and 55 ps for **1d**⊂Ag^{I}. However, the reconstructed spectra of both components overlap largely for all the cations studied (e.g., maximum at 580 nm for the 90 ps species and 584 nm for the 568 ps species in the case of **1d**⊂Hg^{II}). This strong spectral overlap implies a large Stokes shift for this fast decaying component as well and does not favor its attribution to the initially excited (LM)*. Because of limitations of the experimental setup, a faster and further blue-shifted transient species that could be ascribed to (LM)* could not be detected here.

For a better understanding of the photophysics of the chalcone probes, related ICT probe systems from the literature studied by time-resolved absorption (on the subpicosecond time scale) and emission spectroscopy are briefly discussed here. Comparable cation-induced effects (in absorption and emission but

TABLE 4: Spectroscopic Properties of the Cation Complexes of 1c in Acetonitrile[a]

	$\tilde{\nu}$(abs), 10^3 cm^{-1}	$\tilde{\nu}$(em), 10^3 cm^{-1}	$\Delta\tilde{\nu}_{cp-fp}$(abs), cm^{-1}	$\Delta\tilde{\nu}_{cp-fp}$(em), cm^{-1}	ϕ_f	τ_f, ps	log K_S(abs)	log K_S(em)	r_M,[b] Å	n^2/r_MZ^2, Å^{-1}
1c[c]	21.69	15.48			0.007	71				
⊂**Li**^{I}[d]	22.78	15.78	1090	300	0.04	171	2.57	2.42	0.76	1.32
⊂**Na**^{I}	23.07	15.95	1380	470	0.04	102	1.79	1.85	1.02	0.98
⊂**K**^{I}	22.39[e]	15.70[e]	700	220	0.03[e]	87	1.4[e]	n.d.	1.46	0.68
⊂**Mg**^{II}	28.68, 17.30	16.81, −	6990, −4390	1330, −	n.d.[f]	86	n.d.[f]	n.d.	0.72	5.55
⊂**Ca**^{I}[d]	27.89	16.38	6200	910	0.06	192	3.69	3.37	1.06 (7)	3.77
⊂**Sr**^{II}	27.25	16.08	5560	600	0.05	201	2.82	2.82	1.21 (7)	3.31
⊂**Ba**^{II}	26.32	16.02	4630	540	0.03	n.d.	2.80	2.38	1.47 (9)	2.72
⊂**Pb**^{II}	27.93	16.50	6240	1020	0.06	n.d.	n.d.	n.d.	1.19	3.36
⊂**Hg**^{II}, **Cu**^{II}	30.20, 16.83		8510, −4860				n.d.	n.d.	1.02, 0.73	3.92, 5.48

[a] The experiments were carried out up to the millimolar concentration range for alkali and alkaline-earth metal ions and up to the micromolar concentration range for heavy and transition metal ions[164] ($c_L = 3 \times 10^{-6}$ M; short decay components not included; for discussion, see text). [b] All the radii were taken from ref 120 and are for six-coordination except where the coordination number is indicated in brackets.[165] The values given in parentheses have been found by Jonker in X-ray analyses of related MAP-A15C5 (Scheme 2) complexes.[68,165] Cavity size of the aza crown: 1.7−1.8 Å.[124,169] [c] No effects on the ICT band observed for Zn^{II}, Cd^{II}, Ni^{II}, Co^{II}, Cu^{I}, Ag^{I}. [d] Conductometrically determined log K_S: **1c**⊂Li^{I} = 2.80, **1c**⊂Ca^{II} = 3.29. [e] Extrapolated values because full complexation could not be achieved due to solubility problems [f] Excitation at the red-shifted absorption band does not yield any measurable fluorescence; ϕ_f and log K_S have not been determined because full complexation could not be achieved. Additionally, the low-energy absorption and emission band largely overlap.

TABLE 5: Spectroscopic Properties of Some D−A-Chalcones in Acetonitrile in the Presence of Mg^{II}, Hg^{II}, and H^+

	$\tilde{\nu}$(abs)^{blue}, 10^3 cm^{-1}	$\tilde{\nu}$(abs)^{red}, 10^3 cm^{-1}	$\tilde{\nu}$(em), 10^3 cm^{-1}	$\Delta\tilde{\nu}_{cp-fp}$(abs)^{blue}, cm^{-1}	$\Delta\tilde{\nu}_{cp-fp}$(abs)^{red}, cm^{-1}	rel fl[a]
1d[b]		21.98	15.70			
⊂**Hg**^{II}	29.3		17.00	7320		E
1c[b]		21.69	15.48			
⊂**Mg**^{II}	28.68	17.30	16.81	6990	−4390	E
⊂**Hg**^{II}	30.20	16.83		8510	−4860	
1a		21.83	15.22			
⊂**Mg**^{II}		17.45			−4380	
⊂**Hg**^{II}		16.83			−5000	
H^+	30.30		19.61	8470		Q
1b[c,d]		29.67	23.29			
1f[e]		27.10	19.61			
⊂**Hg**^{II}		22.22			−4880	
2c		24.27	18.50			
⊂**Mg**^{II}	31.54	(21.19)	18.76	7270	(−3080)	Q
2a[f]		24.51	18.45			
⊂**Mg**^{II}		21.19			−3320	
3[f]		23.09	15.62			
⊂**Mg**^{II}		18.15			−4940	

[a] In the case of the relative fluorescence an "E" denotes enhancement and a "Q" denotes quenching. [b] The effects observed for protons are similar to those of **1a**. [c] Similar effects for **2b**. [d] No effects for Mg^{II}, Hg^{II}, H^+. [e] No effects for H^+. [f] The effects observed for protons and Hg^{II} are similar to those of **1a**; in the case of Hg^{II}, only stronger for **3** and weaker for **2a**.

TABLE 6: ^{1}H NMR Chemical Shifts δ (ppm from TMS) of 1a, 2a, and 3 and the Respective Mg^{II}-Induced Shifts Δ (ppm; solvent = CD_3CN, Counterion = Perchlorate, $c_L = 1.5 \times 10^{-3}$ M, $c_{Mg} = 0.27$ M; D, A = Molecular Fragments; Additional Chemical Shifts $\Delta = \delta_{cp} - \delta_{fp}$; Δ Shifts)

		1a		**3**		**2a**	
position		δ	Δ	δ	Δ	δ	Δ
D	DMA	3.047	0.035	3.035	0.084	3.012	−0.001
	ortho	6.778	0.027	6.791	0.051	6.756	−0.003
	meta	7.680	0.060	7.689	0.155	7.617	0.008
	α	7.997	0.126	8.289	0.056	7.716	0.034
	β	7.800	−0.175	7.886	0.026	7.464	−0.005
A	2					8.027	0.000
	3			8.189	0.388	7.516	−0.014
	4	8.197	0.040	8.434	0.314	7.595	0.013
	5	7.575	0.047	8.004	0.129		
	6	7.630	0.048	7.710	0.106		
	7	8.104	0.047	7.859	0.099		
	8			8.243	0.230		

involving fluorescence quenching) have been reported for stilbene- and merocyanine-like DCS-A15C5 and DCM-A15C5 (Scheme 2).[9−12] For both probes, fast decay components were found at the high-energy side of the complex's emission band (e.g., 400 ps in the case of DCM-A15C5⊂Ca^{II}; τ_f (DCM-A15C5) = 2.1 ns).[9,11,12] Furthermore, subpicosecond transient absorption measurements (Martin et al. for DCM-A15C5 and Rullière et al. for DCS-A15C5) revealed that another species showing a strongly hypsochromically shifted emission spectrum is involved in the excited-state process on the femtosecond time scale (<2 ps for DCM-A15C5; similar lifetimes have been reported for DCS-A15C5).[9−12] In these complexes, excitation leads to initial formation of (LM)* with strong cation−probe interaction followed by an ultrafast "internal dissociation" (<700 fs for M^{n+}⊂DCM-A15C5), yielding the excited cation−probe contact pair (L*M). Reorientation of the solvation sphere finally results in formation of a ternary complex (L*/S/M) where the coordination site of the cation formerly inhabited by the crown nitrogen atom is now occupied by a solvent molecule (S).[11,12] The latter process occurs on the picosecond time scale and depends on the coordinating ability of the cation; i.e., (L*/S/M) formation is observed within 2 ps for Li^{I}⊂DCM-A15C5 and 30 ps for Ca^{II}⊂DCM-A15C5, respectively.[9,10] The fluorescence of this latter species decays with a lifetime of ca. 1.9 ns (for the cation complexes of DCM-A15C5) and displays the spectral features of the steady-state emission spectrum.

Transferring this model to our observations confirms the suggestion that detection of locally excited (LM)* escapes the limited temporal resolution of our instrument and the fast decay component found for **1c**⊂Ca^{II} and **1d**⊂Ag^{I}/Hg^{II} is attributed to the loose contact pair (L*M). After reorientation in the cation's coordination sphere, the main emissive species (L*/S/M) is formed and emits with its characteristic lifetime τ_2, e.g., 348 ps in the case of **1d**⊂Ag^{I} (Table 3), the value of the latter lifetime reflecting the coordinative strength of the cation best (e.g., τ_2(**1d**⊂Hg^{II}) > τ_2(**1d**⊂Ag^{I}) and see the log K_S values in Table 3). The formation of an outer sphere complex (i.e., complete cation ejection from the aza crown), a much slower process itself,[10,115] does not seem to be operative here.

Case of ***1d*****⊂*Hg^II*.** For **1d**⊂Hg^{II}, two largely overlapping species with fluorescence lifetimes in the (sub-)nanosecond time range (568 and 1070 ps) and comparable amplitudes are found (for $DAS_i(\lambda)$ ratios, see caption to Figure 11 and ref 116). However, evaluation of the global analysis results assuming a simple three-state reaction scheme[84] does not yield satisfactory results neither for a consecutive (A → B → C) nor for a parallel (B ← A → C) reaction mechanism. Thus, another rearrangement in the complex during its excited-state lifetime (according to a consecutive reaction mechanism (L*M) → $(L^*/S/M)_1$ → $(L^*/S/M)_2$) can be excluded as well as the formation of two different loose complexes from a single precursor species in a parallel reaction mechanism, $(L^*/S/M)_2$ ← (L*M) → $(L^*/S/M)_1$. Moreover, the UV/vis-spectrophotometric titrations reveal a constant decrease (increase) of the absorption band of the free probe (complexed probe) up to $x_{M/L} = 1$, suggesting only the formation of a 1:1 complex. A possible explanation, which however lacks experimental verification here,[111] is the occurrence of two ground-state complexes in differing conformations, L + M → $LM_A \rightleftharpoons LM_B$ (a well-known fact for crown ether receptors; see, for instance, ref 19).[117] In such a case, when both complexes show largely overlapping bands, simultaneous excitation leads to two different excited species $(L^*M)_A$ and $(L^*M)_B$ undergoing parallel decoordination reactions ($(L^*M)_A$ → $(L^*/S/M)_A$ and $(L^*M)_B$ → $(L^*/S/M)_B$) on a similar time scale and hence four decay components should be noticed (In this case, all the data obtained by steady-state spectroscopy are average values of both conformers weighted by their relative concentrations and, since both conformers exhibit a 1:1 stoichiometry, sharp isosbestic points can still be observed.).[19] Analysis of the fluorescence decay curves with four components improves the fit to a minor extent but does not yield reliable results concerning a possible model. Another explanation may involve a second chelating site in the chromophore although its direct detection was not possible for **1d**⊂Hg^{II} by employing optical spectroscopy (see section 3.10 for discussion). Thus, the real nature of the dynamic emission behavior of the Hg^{II} complex(es) remain(s) obscure at present.

3.9. Complex Stability Constants and Spectroscopic Effects. *Correlation of Cation-Induced Spectral Shifts and Charge Density.* In the ground state, the size of the chelation-induced blue shift of the ligand absorption band reflects the reduction of the electron donating character of the nitrogen atom of the monoaza crown due to cation coordination. Thus, it depends on the charge density and electron affinity of the cation bound, the strongest changes occurring for Hg^{II} (**1d**) and for monovalent Na^{I} and divalent Mg^{II} (**1c**; cf. resemblance of the absorption spectra of **1b** and the complexes in Figures 8 and 12). For **1c**, the same order is found as has been reported for other probes such as DCS-A15C5,[12,17] DCM-A15C5,[15] and MAP-A15C5[68] (Scheme 2). The size of the complexation-induced shifts in absorption decreases on the order of Mg^{II} > Ca^{II} > Sr^{II} > Ba^{II} ≫ Na^{I} > Li^{I} (>K^{I}) whereas for the stability constants of the complexes, an order of Ca^{II} ≫ Sr^{II} > Ba^{II} > Li^{I} ≫ Na^{I} > K^{I} occurs (Table 4; in the case of Mg^{II}, log K_S could not be determined spectroscopically.). The good correlation observed for a plot of the cation-induced spectral shifts $\Delta\tilde{\nu}_{cp-fp}$(abs) and the complex stability constants log K_S vs the so-called class A or ionic index (ratio of charge and ion radius n^2/r^{n+} as a measure for electrostatic attraction)[118] shown in Figure 13 suggests that for a chosen ICT probe both effects depend mainly on electrostatic interaction.

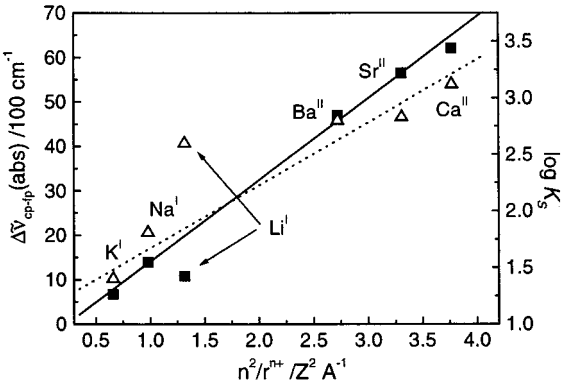

Figure 13. Cation-induced shift in absorption $\Delta\tilde{\nu}_{cp-fp}$(abs) (—, ■) and log K_S (···, △) as a function of charge density (class A index) for **1c** and its alkali and alkaline-earth metal ion complexes in acetonitrile. Fits do not contain the value for Li^{I}.

However, an exceptional behavior is observed for Li^{I} (Figure 13). Because of its higher charge density, $\Delta\tilde{\nu}_{cp-fp}$(abs) should be larger for Li^{I} compared to the value found for Na^{I}. Instead, the opposite is noticed. On the other hand, Li^{I} shows a complex stability constant higher than that of Na^{I}. This is in agreement with the Pearson hardness parameter[32,33] but seems to contradict a second quantity affecting the stabilization of macrocyclic complexes, the optimum fit of the cation into the receptor's cavity.[119] Na^{I} (ionic diameter of 2.04 Å for a coordination number of 6) fits considerably better into the A15C5 cavity (1.7−2.2 Å) than Li^{I} (ionic diameter of 1.52 Å for a coordination number of 6).[120] This suggests that coordination of Li^{I} most likely involves only the four macrocyclic oxygen atoms while the other two coordination sites of the cation are saturated with oxygen atoms of the counterion and/or solvent molecules. This is consistent with X-ray data of the metal ion complexes of MAP-A15C5 derivatives reported by Jonker et al. and Heijdenrijk et al. where the distance between the nitrogen atom of the crown and the cation decreases on the order of K^{I} > Li^{I} > Na^{I}.[25,68,69] Furthermore, extraction experiments carried out for 15C5 by Iwachido et al. reveal that 15C5⊂Li^{I} is extracted as a dihydrate (2.0 water molecules per complex molecule, four coordinative bonds to only four donor oxygens) whereas, for 15C5⊂Cs^{I}, coextraction of only 0.2 water molecules occurs.[121]

For the alkaline-earth metal ions, all the tendencies discussed correlate well (spectral shifts, K_S values, n^2/r^{n+}), the enhanced K_S value for Ca^{II} compared to those for Sr^{II} and Ba^{II} stressing the optimum fit of this cation into the cavity of the receptor.

*A15C5 Receptor (**1c**).* The single factors governing the absolute values of log K_S for the Ph-A15C5 receptor unit in the ICT probe molecules have been discussed by Fery-Forgues et al. for BOZ-A15C5 (Scheme 2) and DCM-A15C5[122] and by us for a series of 35 different ICT probes.[13] The interplay between the degree of conjugation in the whole chromophore (orbital overlap between aniline nitrogen and aniline phenyl ring

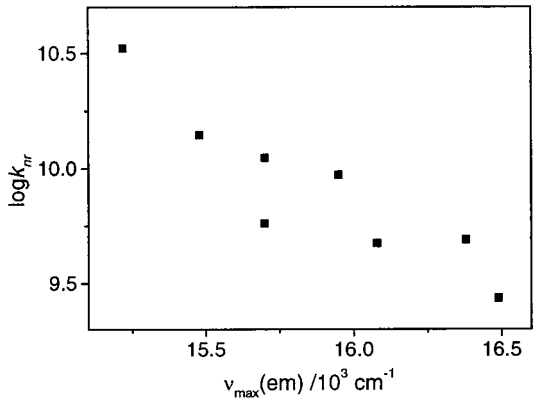

Figure 14. Plot of log k_{nr} vs $\tilde{\nu}$(em) for **1a**, **1c**, and **1d** as well as the Na^I, K^I, Ca^{II}, and Sr^{II} complexes of **1c** and the Ag^I complex of **1d** in acetonitrile.

due to the twist between the fragments and/or pyramidalization at the nitrogen atom) and the inductive effect of the para substituent of the aniline moiety, i.e., the basic chromophore, accounts for the fact that the correlation between complex stability and spectroscopic and NMR data is not straightforward. However, Fery-Forgues et al. found an empirical relationship linking the $\Delta(Ca^{II})$ shifts of the ^{1}H NMR signals of the ortho and meta protons to the complex stability constants for a series of para-substituted Ph-A15C5 derivatives.[122] Using this relationship (eq 10), a value of log $K_S = 3.67$ is calculated for **1c**$\subset Ca^{II}$, in good agreement with the experimentally found value of 3.69 (Table 4; for NMR data, see Tables 6 and S7).

$$\log K_S = 1.79(\pm 0.17) + 5.36(\pm 0.59)[\Delta(Ca^{II})_{ortho} - \Delta(Ca^{II})_{meta}] \quad (10)$$

*$AT_4$15C5 Receptor (**1d**).* Although the complex stability constant of **1d**$\subset Ag^I$ is even larger than those observed for the divalent alkaline-earth metal ions (Tables 3 and 4), the shift in absorption of 900 cm^{-1} found for Ag^I is rather small. This behavior stresses the high preference of Ag^I for sulfur donor atoms that has been also described for other dithia diaza crown ethers.[123] In the case of Hg^{II} showing both a stronger coordination to nitrogen donor atoms and a higher charge density, the spectral shifts are much more pronounced.

Cation-Induced Fluorescence Enhancement. In section 3.6, the fluorescence emission of D−A-chalcones in highly polar solvents has been attributed to the population of a highly polar, single bond twisted transient species A* (with possible competition of nonemissive K*-state formation). Moreover, in these solvents the involvement of a nonemissive P* state was found to be of minor importance for **1c** and **1d**, respectively. As in the free probes, the single bonds are unbridged in the complexes and thus population of A* (and K*) should be possible as well. Moreover, under the assumption that rotation around the double bond b_{67} (toward P*) is negligible, the bulkiness of the complexed receptor should considerably slow rotational motions around all the single bonds. For the uncomplexed dyes **1a** and **1c**−**e**, the observed decrease in fluorescence quantum yield and lifetime was mainly attributed to the S_1-S_0 energy gap[106] (Figure 7, discussion in section 3.6) and k_{ic} ($k_{nr} \sim k_{ic}$) and the complexed probes should show a comparable correlation as follows from Figure 14.[88] Under the assumption that the influence of all the other possible excited-state deactivation routes is negligible and the rate constant for K*-state formation is comparable for the complexes, this leads to the conclusion that the cation-induced fluorescence enhancement can be predominantly attributed to a change in donor strength, i.e., to a complexation-induced blue shift in emisson, and does not seem to involve the blocking off or slowing down of excited-state reactions connected with a specific rotational motion. Moreover, in the case of **1d**$\subset Hg^{II}$, enhanced spin−orbit coupling due to the heavy atom effect does not seem to play a major role as well.

*Comparison of **1d** and **1c**.* Upon exchanging the macrocyclic sulfur heteroatoms for oxygen, the negative charge of the heteroatoms increases and thus the electrostatic attraction between the heteroatoms and the "hard" alkali or alkaline-earth metal cation via ion−dipole forces is enhanced, resulting in complexation of these ions. On the contrary, for "soft" Ag^I and Hg^{II} (with a high class B or covalent index) the effects are opposite; i.e., less electrostatic but rather covalent bonding is involved, especially with the nitrogen atom.[124,125] The preferences of a "soft" and a "hard" cation for certain types of donor atoms are well-reflected by the results of the X-ray investigations (section 3.1). The longer distance between Ca^{II} and the nitrogen atom in Ph-A15C5 as compared to Ag^I and the corresponding atom of Ph-$AT_4$15C5 suggests that the stronger shift in absorption seen for Ca^{II} is not due to a stronger interaction but due to the higher charge density of this divalent ion compared to monovalent Ag^I.

Upon comparison of **1c** and **1d** with other ICT probes, the increase in both fluorescence quantum yield (factors 2−8) and lifetime (140−630%) is remarkable and has so far only been reported for very few ICT fluorescent probes,[65,128] for instance, for related BOZ-A15C5 (factor of 2 in ϕ_f and 160% increase in τ_f).[65] Even more interestingly, these features are preserved upon complexation of **1d** to the well-known fluorescence quencher Hg^{II}. To the best of our knowledge **1d** is the first "classical" ICT probe that shows fluorescence enhancement upon Hg^{II} ion binding. Thus, it should be possible in principle to design intrinsic ICT probes showing chelation-enhanced fluorescence even for such heavy and transition metal ions.

3.10. Nature of the Complexes and Cation Selectivity. For a better understanding of the spectroscopic behavior of **1c**$\subset Mg^{II}$ and the reactions with some heavy and transition metal ions, the complexation behavior of other D−A-chalcones without a receptor was also investigated. For fluorescent probes with a benzothiazole acceptor, complex formation via a second coordination site in the acceptor part of the molecule is possible (Scheme 4). This yields a bidentate chelate with a five-membered ring structure involving both the oxygen atom of the carbonyl group and either the sulfur or the nitrogen atom of the benzothiazole ring (cf. syn/anti stereoisomerism discussed above). All the potential cation coordination sites and structures of the resulting complexes follow from Scheme 4 and include routes A, B, and C (**1c** **1d**), B and C (**1a**, **1b**, **1f**, **6**), A (**2c**), or B (**3**). For **2a** and **2b**, no complex formation according to routes A, B, and C is possible and only loose coordination of an ion to the carbonyl oxygen atom can occur (or protonation of the amino group in **2a**). The complexation of **1a**, **1b**, **1f**, **2a**−**c**, **3**, and **6** with Mg^{II}, Hg^{II}, Cu^{II}, Zn^{II}, Ni^{II}, Pb^{II}, and H^+ was studied via absorption and emission measurements. Additionally, ^{1}H NMR investigations of **1b** **1c**, **2a**, and **3** in the presence of Mg^{II} and Ca^{II} were carried out.

Complexes of Hg^{II} and Mg^{II}. Figure 15 combines the UV/vis-spectrophotometric titration spectra of **1a** with Hg^{II} (for a comparison with **1d** and Hg^{II}, see Figure 9). The absorption spectra of **1a**, **2a**, **2b**, and **3** in the presence of a large excess of Mg^{II} are displayed in Figure 16. Other relevant spectroscopic data are included in Table 5.

SCHEME 4: Potential Coordination Sites in D−A-Chalcones Containing a Benzothiazole Acceptor and a Monoaza Crown Ether Donor[a]

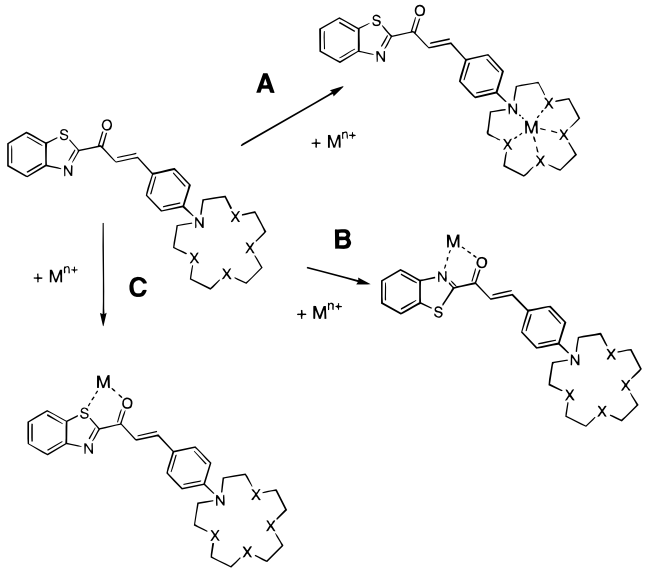

[a] Formation of the ion−macrocycle complex (route A), a N,O-chelate (route B) or a S,O-chelate (route C) (formation of a five-membered S,O-chelate (route C) is considered as being more or less only theoretically possible).

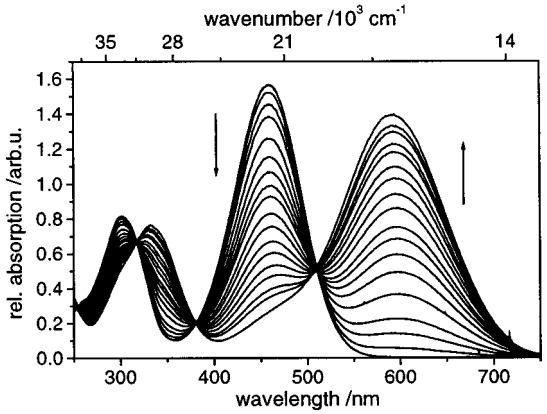

Figure 15. UV/vis-spectrophotometric titration spectra of **1a** with Hg^{II} perchlorate in acetonitrile ($c_L = 9 \times 10^{-6}$ M, Hg^{II} addition in the range of $0.04 \leq x_{M/L} \leq 20$).

As follows from the titrations shown in Figures 9 and 15, the shifts induced by Hg^{II} are clearly different for **1a** and **1d**, suggesting a second coordination site being operative here. However, protonation of both dyes similarly leads to abstraction of the nitrogen lone electron pair and thus to an absorption band resembling that of **1b** (Table 5). The appearance of a new red-shifted absorption band for **1a**⊂Hg^{II} indicates an increase of the ICT character, i.e., an increase in acceptor strength for this complex. Moreover, the electronic nature of the Hg^{II} ion (closed-shell d^{10} configuration) and the high molar absorptivity of the red-shifted band ($\epsilon \sim 31\,000$ M^{-1} cm^{-1}) excludes any ligand field transitions. Formation of such an acceptor-based chelate is further supported by comparison of the protonation and Hg^{II} complexation data of **1a** and **1f**, which differ in the donor part (**1a**, dimethylamino; **1f**, methoxy). In the absence of a nitrogen-containing amino group, no hypsochromic shifts are observed upon addition of protons (0.1 M $HClO_4$). In contrast, addition of Hg^{II} induces very similar bathochromic shifts of 4900 cm^{-1} for both compounds (Table 5), confirming the formation of an

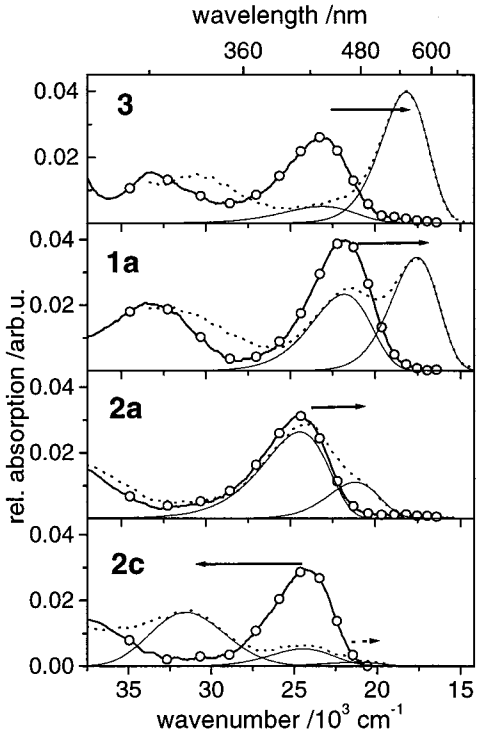

Figure 16. Steady-state absorption spectra of **3**, **1a**, **2a**, and **2c** in the absence and the presence of a high excess of Mg^{II} ($x_{M/L} = 85\,000$, $c_L = 1 \times 10^{-6}$ M, ○ = free dye, ••• = complex, — = single components). The spectra were fitted by modeling the band of the free dye and including one (or two in the case of **2c**) additional band(s) as log-normal function(s). In the case of **2c** and Mg^{II}, a weak shoulder at the low-energy edge of the absorption band was also found at this high cation excess. The arrows denote the shifts observed.

acceptor-based chelate. These findings are in good agreement with the results obtained for the main group metal ion Mg^{II} and various D−A-chalcones (Figure 16). As follows from Figure 16, the appearance of a red-shifted band is obviously connected to the presence of a heteroatom in the aromatic acceptor part of the chalcones. **3**, mimicking closely the M^{n+}-favored chelating reagent 8-hydroxyquinoline (8-HQ),[129] shows the most pronounced effect, i.e., the largest increase in the red-shifted band and, correspondingly, the largest decrease of the free dye's absorption band (reduced to ca. one-fifth of its initial intensity). Additionally, the bathochromic shift observed is the strongest for this series of D−A-chalcones (4940 cm^{-1}). **1a**, carrying the benzothiazole moiety with a heterocyclic nitrogen atom of reduced basicity, is a weaker coordination site and shows a smaller effect at the same ion concentration.[130] In the case of **2a** and **2c** lacking a heterocyclic nitrogen atom in the phenyl acceptor, only coordination to the carbonyl oxygen atom can induce a bathochromic shift. As follows from Figure 16 coordination of Mg^{II} to the carbonyl group leads to a change in absorption. However, this effect is rather weak because the formation of a stabilizing bidentate chelate is not possible. Furthermore, exchanging the DMA for an A15C5 group (**2a** → **2c**) yields the "normal" complexation behavior observed for the other alkaline-earth metal ions and **1c**, i.e., a cation-induced hypsochromic shift of the absorption band. Only a very weak, red-shifted shoulder is seen in the spectrum of **2c**⊂Mg^{II}. Similar effects, i.e., complexation-induced red shifts in absorption upon coordination to a carbonyl group in the acceptor part of a molecule, have been observed for coumarin-[23] and flavonol-based[131] fluorescent probes as well as for a closely related fluorescent probe of the diphenylpentadienone type.[132]

For **1b**, **2b**, and **6**, no spectroscopic changes are observed in any case. However, this does not necessarily imply that no chelate formation occurs but that such a product is not spectroscopically detectable. Here, as in many other complexes of diamagnetic (main) group metal ions, the absorption and emission spectra of the possible complexes should closely resemble those of the free ligand.[133]

In the case of **1d**$\subset Hg^{II}$ additional coordination in the acceptor part of the complex may also account for its time-resolved emission behavior (see section 3.8), i.e., the occurrence of (at least) three decay components. Since binding of Hg^{II} to the receptor blocks off the ICT process, the consecutive M_2L complex might escape UV/vis-spectrophotometric detection.[134] Moreover, when comparing the relative amplitudes[135] found in a time-resolved fluorescence experiment for the 1.1 ns component at $x_{M/L} = 1$ and $x_{M/L} = 10$, the values of 0.48 ($x_{M/L} = 1$) and 0.42 ($x_{M/L} = 10$) indicate no drastic changes.[136] Also, the M_2L complex can be nonfluorescent.

Complexation Involving Cu^{II}. The results obtained during the Cu^{II} binding studies led to some additional investigations involving Ph-$AT_4$15C5 and Ph-A15C5. Addition of Cu^{II} to the former in acetonitrile leads to the disappearance of the two lowest transitions at 38 500 cm^{-1} ($\epsilon \sim 17\,800\ M^{-1}\ cm^{-1}$) and 33 100 cm^{-1} ($\epsilon \sim 2200\ M^{-1}\ cm^{-1}$), respectively, and the formation of new absorption bands centered at 38 700 cm^{-1} (m), 29 100 cm^{-1} (m), 23 000 cm^{-1} (m), and 17 600 cm^{-1} (w), respectively.[137] In accordance with other data published on the electronic spectra of Cu^{II} thioether coordination compounds, the two low-energy bands are assigned to $\sigma(S) \rightarrow$ Cu LMCT as well as (probably superimposed) $\pi(S) \rightarrow$ Cu LMCT and/or d−d* ligand field transitions. For $AT_4$15C5, Westerby et al. reported bands at 24 100 cm^{-1} ($\epsilon = 6100\ M^{-1}\ cm^{-1}$) and 18 700 cm^{-1} ($\epsilon = 1900\ M^{-1}\ cm^{-1}$)[138] and in comparable thia crown ethers, the $\sigma(S) \rightarrow$ Cu LMCT transitions are located in the same spectral regions.[139] The latter band centered at ca. 17 200 cm^{-1} is assigned to various transitions of $\pi(S) \rightarrow$ Cu LMCT and/or d−d* ligand field type.[142−144]

A UV/vis-spectrophotometric titration of **1d** with Cu^{II} shows that up to $x_{M/L} = 1$, the bands of the free probe (33 200 and 21 900 cm^{-1}) are diminished and new bands at 31 900 cm^{-1} (s) and 16 700 cm^{-1} (m) are observed.[145] In the course of the titration, these bands decrease and the bands at 23 900 cm^{-1} ($\epsilon = 2400\ M^{-1}\ cm^{-1}$) and 18 100 cm^{-1} ($\epsilon = 2000\ M^{-1}\ cm^{-1}$) (at full complexation) build up. Because of the strong overlap of Cu^{II} thioether or Cu^{II} amine bands with those of the chromophore, assignments of the higher energy absorption bands were not possible. Having in mind the possible formation of acceptor-based chelates (band centered at 16 900 cm^{-1} for Hg^{II}) and the occurrence of sulfur−Cu^{II} transitions, a partly consecutive and partly parallel formation of a chelate and a macrocyclic inclusion complex is anticipated. This is further supported by the comparatively low complex stability constant of $\log K_S = 3.86$ for $AT_4$15C5$\subset Cu^{II}$.[138]

The situation is even more complicated for **1a** and Cu^{II}. Here, in a complexometric titration, four different regions are observed, i.e., $x_{M/L} \leq 0.5$, $0.5 < x_{M/L} \leq 1$, $1 < x_{M/L} \leq 3$, and $3 < x_{M/L}$.[145] For the first two regions, the typical chelate band at ca. 16 700 cm^{-1} is observed, but upon further increasing the Cu^{II} concentration, a band at 30 800 cm^{-1} and several strongly overlapping bands (various shoulders in the range of 28 600 to 14 300 cm^{-1}) were found. Although the results obtained for Ph-A15C5 and **2a** point to coordination of Cu^{II} to the DMA group, for **1a** the assignment of any of these bands was impossible due to their strong overlap.[146] Moreover, no effects were found in a UV/vis-spectrophotometric titration of **1b** and **2b** with Cu^{II}. Titrations performed with **1f** (donor does not contain a nitrogen atom) and Cu^{II} support these findings; i.e., a sharp isosbestic point is observed and both the decrease as well as increase of the bands at 27 100 and 22 200 cm^{-1} are similar to those found in a titration of **1f** and Hg^{II}. Here, no other coordination site interferes in Cu^{II} titration.

Comparing the molar absorptivities and size of the blue- and red-shifted absorption bands of the Hg^{II} and Cu^{II} complexes of **1d** and **1a**, respectively, it is obvious that Hg^{II} coordinates (mainly) to the donor in the former and to the acceptor in the latter but Cu^{II} shows mixed coordination for both compounds, possibly involving a rearrangement of the complexes as well.

Complexation Involving Cu^{I}. For any of the chalcone derivatives studied, Cu^{I} induces no spectral shifts. However, in the case of **1d**, complexation is anticipated in agreement with other literature systems[147−149] but lacks spectroscopic detection. For several other polythia crown ethers, Cu^{I} complexation was observed the complex geometry preferably being tetrahedral.[148] Corfield et al. observed tetrahedral coordination for $T_5$15C5$\subset Cu^{I}$ with the remaining fifth sulfur donor atom lacking any binding to the central ion.[149] Even for macrocyclic dithia diaza ligands of different ring sizes, exclusive thioether coordination of Cu^{I} was reported.[147] With respect to **1d** this suggests that complexation occurs but no spectral shifts occur due to the absence of Cu^{I} nitrogen interaction.[150] Furthermore, the possibilities to detect any Cu^{I} thioether MLCT transitions in the absorption spectrum are poor because such absorption bands appearing in the region of 43 500−33 300 cm^{-1} should strongly overlap with the intense absorption of the organic probe molecule.[151]

Complexation Involving Other Metal Ions. Only at higher concentrations (at $x_{M/L} \geq 5$) is a behavior similar to that of the "red" Mg^{II} complex observed for the other heavy and transition metal ions such as Zn^{II}, Ni^{II}, and Pb^{II}. As compared to Mg^{II}, the smaller amounts of these ions required to induce similar effects correlate well with the generally higher complex stability constants of these ions in chelates of such a type[129,130,152] and is also expressed by the relatively high class A or ionic index of these ions (Tables 3 and 4). Moreover, the presence of only a single nitrogen in the receptor sufficiently prevents complexation of those transition metal ions that show pronounced preference for nitrogen donor atoms, e.g., Zn^{II} and Ni^{II}, at this binding site.[153] This lack of coordination to **1c** and **1d** is exemplified by the absence of a blue-shifted band for **1a** in the prescence of these ions. For Pb^{II} and **1d**, complexation is not favored despite the high class B index of this ion (Table 3).[118] Instead, the exchange of oxygen for sulfur donor atoms leads to enhanced binding selectivities for the "soft" metal ions Ag^{I} and Hg^{II} compared to Pb^{II}, possessing borderline character.[32,154] Similar observations have been made for a large number of mixed mono- or diaza polyoxa/thia crown ethers.[155,156] Here, in all cases, binding to Pb^{II} (as well as Cd^{II} and Co^{II}) is much weaker than complex formation with Cu^{II} and Ag^{I}.[155] Furthermore, only in the case of Pb^{II} did alkylation of the nitrogen donor atoms result in a significantly lower complex stability constant.[155]

Complexation to A15C5 leading only to the "normal" effect (route A in Scheme 4) in the case of the other alkaline-earth metal ions besides Mg^{II} can be rationalized in terms of the complexation behavior of 8-HQ, which binds Mg^{II} with a much higher complex stability constant.[152]

NMR Spectroscopic Study of Mg^{II} and Ca^{II} Complexes. To obtain more information about the chemical structure of the Mg^{II} and Ca^{II} complexes of **1a**, **1c**, **2a**, and **3**, ^1H NMR spectra of

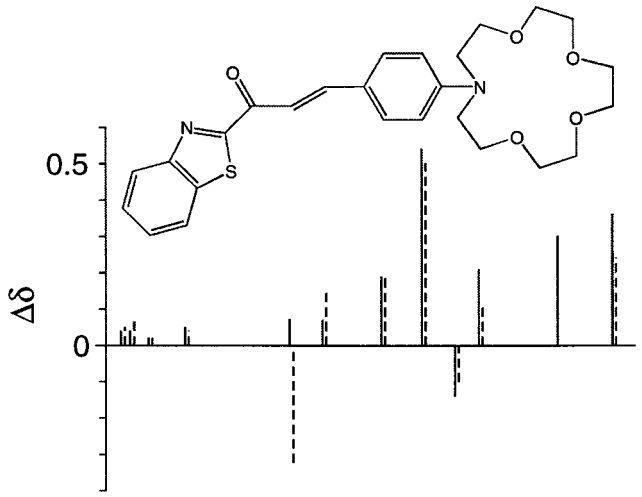

Figure 17. Graphical representation of the Δ shifts induced by Ca^{II} (—) and Mg^{II} (---) at the corresponding proton positions of **1c** (solvent = CD_3CN, counterion = perchlorate, $c_L = 1.5 \times 10^{-3}$ M, $c_{Ca} = 0.30$ M, $c_{Mg} = 0.27$ M).

these compounds were recorded in the absence and presence of Mg^{II} and Ca^{II} perchlorates in CD_3CN, respectively. In contrast to optical spectroscopy, complex formation and dissociation are comparatively fast on the NMR time scale and thus the chemical shifts measured are only average values. Also, the additionally observed shifts are not directly related to the strength of the complex formed.

The data follow from Tables 6 and S7, respectively. The Δ shifts are comparatively small for **2a** and Mg^{II}, but especially in the case of **3**, strong shifts to lower field are observed for the aromatic protons adjacent to the quinoline nitrogen atom, i.e., H-3, H-4, and H-6. This supports the proposed formation of a bidentate acceptor N,O-chelate (five-membered ring chelate). However **1a**⊂Mg^{II} does not show such pronounced shifts of the BT protons. Here, only the proton signals of H-α and H-*β* of the −CO−CH═CH fragment are shifted in opposite directions, suggesting a dominant interaction of Mg^{II} and the carbonyl oxygen atom. Having in mind the results obtained for **2a** (smaller changes upon addition of Mg^{II}) and the optical effects (Figure 16), this explanation is contradictory. Coordination of Mg^{II} only via the carbonyl group of **1a** is astonishing as the adjacent electrophilic BT moiety should decrease the electron density of the carbonyl oxygen atom and should thus reduce its coordinating ability in **1a** compared to **2a** (and hence, the shifts in the ^1H NMR spectra should be more pronounced for **2a**). A comparison of the complexation behavior of **1a** and **3** shows that, in the former case, complex formation is possible without further rotation of the BT moiety (syn conformation of the N,O-chelate, low rotational barrier), whereas the quinoline ring of **3** has to adopt the less favored syn conformation prior to complexation (in the anti conformation, the steric hindrance of H-3 and H-α is minimized). Accordingly, N,O-chelation takes place in both **1a** and **3**, but the conformational reorientation induces stronger shifts for **3**.

In accordance with the absorption effects, addition of Mg^{II} to **1c** also leads to similar Δ shifts for H-α and H-*β*, suggesting the formation of a N,O-chelate here as well. However, a comparison of the data presented in Figure 17 and Table S7 for **1c**⊂Mg^{II} and **1c**⊂Ca^{II} provide additional evidence for a second, "normal" coordination site in **1c**⊂Mg^{II}. For both, Mg^{II} and Ca^{II}, drastic shifts are observed for the signals of the methylene groups of the crown ether moiety (with opposite signs for the methylene group adjacent to the nitrogen atom) and for those of the aromatic protons in ortho position, but in the case of Ca^{II}, only minor shifts are observed for the vinylenic protons (with an opposite sign for H-α, Figure 17 and Table S7). However, some of the signals are broadened for **1c**⊂Mg^{II}, indicating slow exchange kinetics.

4. Concluding Remarks

The presented studies of the benzothiazole-substituted chalcones reveal that the modified and enlarged excited-state reaction scheme discussed for D−A-stilbenes[103] is consistent with both the phenyl-substituted[79] and the heterocyclic D−A-chalcones, including stronger stabilization of the polar states with increasing solvent polarity for the latter compounds with a stronger acceptor moiety. Although displaying spectrally very similar properties, substitution of the heteroatoms in a crowned anilino donor unit can entail crystallization in very different conformations and allows us to fine-tune the charge transfer process while largely maintaining the size of the donor unit. Emission in polar protic solvents (alcohols) occurs on the same time scale as solvent relaxation for all the D−A-chalcones investigated. But whereas the dynamic emission behavior is straightfoward in highly polar aprotic solvents, the interpretation of the nonexponential decay data in medium and apolar solvents of the D−A-chalcones requires further investigations, preferably time-resolved emission studies of differently bridged derivatives of **2a**.

The enormous potential of carefully directed receptor design for the development of highly cation-selective fluorescent probes clearly follows from a comparison of **1c** and **1d**, differing only in the receptor part. The choice of $AT_4$15C5 not only leads to an increased cation selectivity but additionally to analytically more favorable spectroscopic properties, i.e., higher fluorescence quantum yields and lifetimes while maintaining the cation-induced fluorescence enhancement factors even for the fluorescence quencher Hg^{II}. For both probes, the dynamic working range covers 1−3 orders of magnitude for a conventional steady-state fluorometric titration and can be further increased by a factor of ca. 5 by employing time-resolved fluorometry.[157] In the case of **1d**, simultaneous determination of Ag^I and Hg^{II} is possible by employing time-resolved fluorometry due to their sufficiently different fluorescence decay times ($\tau(3)_{\mathbf{1d}\subset Hg} = 3 \times \tau(2)_{\mathbf{1d}\subset Ag} = 4\tau_{\mathbf{1d}}$ and $\tau(2)_{\mathbf{1d}\subset Hg} = 1.6 \times \tau(2)_{\mathbf{1d}\subset Ag} = 3.3\tau_{\mathbf{1d}}$). Furthermore, application of **1d** in polar solvents with increased "hardness", e.g., water or methanol, should lead to larger complexation-induced shifts for Ag^I. In methanol, the shift observed in absorption equals 2290 cm^{-1} compared to a value of 900 cm^{-1} in acetonitrile. Accordingly, the complex stability constant should be similar or higher in these solvents lacking nitrogen donor atoms (due to reduced ion−solvent interaction).[158] For Ag^I binding by diaza polyoxa crown ethers such an effect was observed by Cox et al.[159] Although **1c** and **1d** are only poorly water-soluble, introduction of specific substituents to different positions of the phenyl fragment of the benzothiazole moiety should be synthetically feasible without largely changing the photophysical properties.[24,160]

Another aspect that needs careful consideration for future probe design is obviously acceptor complexation. Although in the present case, this type of complexation leads to the formation of nonfluorescent complexes, with the appropriate combination of donor and acceptor substituents, e.g., modified derivatives of **2c**, analytically more valuable effects may be achieved.[16,23,131,161] The development of fluorescent probes showing cation-induced bathochromic shifts in emission while

maintaining (at least partly) their fluorescence quantum yield is of major importance in fluorescent probe design.

Acknowledgment. The authors would like to thank Mrs. G. Zschommler for technical assistance in the conductometric experiments and Mrs. M. Spieles in the spectroscopic studies. Financial support by the Deutsche Forschungsgemeinschaft (DFG: Re 387/8-2) and the Bundesministerium für Bildung und Forschung (BMBF, 13N7120) is gratefully acknowledged.

Supporting Information Available: Syntheses and analytical data, description of temperature-dependent measurements, fluorometer calibration and spectra correction, conductometry, X-ray crystallographic data, spectroscopic data, detailed solvatochromic analysis including seven tables and five figures. This material is available free of charge via the Internet at http://pubs.acs.org.

References and Notes

(1) Krasovitskii, B. M.; Bolotin, B. M. *Organic Luminescent Materials*; VCH: Weinheim, 1988.

(2) *Applications of Fluorescence in the Biomedical Sciences*; Taylor, D. L., Waggoner, A. S., Murphy, R. F., Lanni, F., Birge, R. R., Eds.; Alan R. Liss: New York, 1986. *Biosensors with Fiberoptics*; Wise, D. L., Wingard, L. B., Jr., Eds.; Humana: Clifton, 1991. *Fluorescence Spectroscopy*; Wolfbeis, O. S., Ed.; Springer: Berlin, 1993. *Probe Design and Chemical Sensing*; Lakowicz, J. R., Ed.; Plenum: New York, 1994.

(3) *Fluorescent Chemosensors for Ion and Molecule Recognition*; Czarnik, A. W., Ed.; ACS Symposium Series; American Chemical Society: Washington, DC, 1993; Vol. 538.

(4) Wehry, E. L. In *Practical Fluorescence*; Guilbault, G. G., Ed.; Marcel Dekker: New York, 1990; p 367. Oehme, I.; Wolfbeis, O. S. *Mikrochim. Acta* **1997**, *126*, 177.

(5) Valeur, B. In *Probe Design and Chemical Sensing*; Lakowicz, J. R., Ed.; Plenum: New York, 1994; p 21.

(6) Bissell, R. A.; de Silva, A. P.; Gunaratne, H. Q. N.; Lynch, P. L. M.; Maguire, G. E. M.; McCoy, C. P.; Sandanayake, K. R. A. S. *Top. Curr. Chem.* **1993**, *168*, 223. Czarnik, A. W. *Acc. Chem. Res.* **1994**, *27*, 302.

(7) Löhr, H.-G.; Vögtle, F. *Acc. Chem. Res.* **1985**, *18*, 65. Rettig, W.; Lapouyade, R. In *Probe Design and Chemical Sensing*; Lakowicz, J. R., Ed.; Plenum: New York, 1994; p 109.

(8) de Silva, A. P.; Gunaratne, H. Q. N.; Gunnlaugsson, T.; Huxley, A. J. M.; McCoy, C. P.; Rademacher, J. T.; Rice, T. E. *Chem. Rev.* **1997**, *97*, 1515.

(9) Martin, M. M.; Plaza, P.; Dai Hung, N.; Meyer, Y. H.; Bourson, J.; Valeur, B. *Chem. Phys. Lett.* **1993**, *202*, 425.

(10) Martin, M. M.; Plaza, P.; Meyer, Y. H.; Badaoui, F.; Bourson, J.; Lefevre, J.-P.; Valeur, B. *J. Phys. Chem.* **1996**, *100*, 6879.

(11) Dumon, P.; Jonusauskas, G.; Dupuy, F.; Pée, P.; Rullière, C.; Létard, J.-F.; Lapouyade, R. *J. Phys. Chem.* **1994**, *98*, 10391.

(12) Mathevet, R.; Jonusauskas, G.; Rullière, C.; Létard, J.-F.; Lapouyade, R. *J. Phys. Chem.* **1995**, *99*, 15709.

(13) Rurack, K.; Sczepan, M.; Spieles, M.; Resch-Genger, U.; Rettig, W. *Chem. Phys. Lett.* in press.

(14) Minta, A.; Tsien, R. Y. *J. Biol. Chem.* **1989**, *264*, 19449.

(15) Bourson, J.; Valeur, B. *J. Phys. Chem.* **1989**, *93*, 3871.

(16) Bourson, J.; Pouget, J.; Valeur, B. *J. Phys. Chem.* **1993**, *97*, 4552.

(17) Létard, J.-F.; Lapouyade, R.; Rettig, W. *Pure Appl. Chem.* **1993**, *65*, 1705.

(18) Mateeva, N.; Enchev, V.; Antonov, L.; Deligeorgiev, T.; Mitewa, M. *J. Inclusion Phenom. Mol. Recognit. Chem.* **1995**, *20*, 323.

(19) Kollmannsberger, M.; Rurack, K.; Resch-Genger, U.; Daub, J. *J. Phys. Chem. A* **1998**, *102*, 10211.

(20) Barzykin, A. V.; Fox, M. A.; Ushakov, E. N.; Stanislavsky, O. B.; Gromov, S. P.; Fedorova, O. A.; Alfimov, M. V. *J. Am. Chem. Soc.* **1992**, *114*, 6381. Alfimov, M. V.; Churakov, A. V.; Fedorov, Y. V.; Fedorova, O. A.; Gromov, S. P.; Hester, R. E.; Howard, J. A. K.; Kuz'mina, L. G.; Lednev, I. K.; Moore, J. N. *J. Chem. Soc., Perkin Trans. 2* **1997**, 2249. Lednev, I. K.; Hester, R. E.; Moore, J. N. *J. Am. Chem. Soc.* **1997**, *119*, 3456. Crossley, R.; Goolamali, Z.; Gosper, J. J.; Sammes, P. G. *J. Chem. Soc., Perkin Trans. 2* **1994**, 513. Rurack, K.; Bricks, J. L.; Kachkovskii, A. D.; Resch, U. *J. Fluoresc.* **1997**, *7*, 63S. de Silva, A. P.; Gunaratne, H. Q. N.; McCoy, C. P. *J. Am. Chem. Soc.* **1997**, *119*, 7891.

(21) Valeur, B.; Pouget, J.; Bourson, J.; Kaschke, M.; Ernsting, N. P. *J. Phys. Chem.* **1992**, *96*, 6545. Shen, Y.; Sullivan, B. P. *Inorg. Chem.* **1995**, *34*, 6235. Collins, G. E.; Choi, L.-S.; Callahan, J. H. *J. Am. Chem. Soc.* **1998**, *120*, 1474.

(22) Vo-Dinh, T.; Viallet, P.; Ramirez, L.; Pal, A.; Vigo, J. *Anal. Chim. Acta* **1994**, *295*, 67. Kuhn, M. A.; Hoyland, B.; Carter, S.; Zhang, C.; Haugland, R. P. *Proc. SPIE-Int. Soc. Opt. Eng.* **1995**, *2388*, 238.

(23) Bourson, J.; Badaoui, F.; Valeur, B. *J. Fluoresc.* **1994**, *4*, 275.

(24) Alfimov, M. V.; Fedorov, Y. V.; Fedorova, O. A.; Gromov, S. S.; Hester, R. E.; Lednev, I. K.; Moore, J. N.; Oleshko, V. P.; Vedernikov, A. I. *J. Chem. Soc., Perkin Trans. 2* **1996**, 1441.

(25) Jonker, S. A.; van Dijk, S. I.; Goubitz, K.; Reiss, C. A.; Schuddeboom, W.; Verhoeven, J. W. *Mol. Cryst. Liq. Cryst.* **1990**, *183*, 273.

(26) Rurack, K.; Bricks, J. L.; Slominski, J. L.; Resch, U. *Dyes Pigm.* **1998**, *36*, 121.

(27) Rurack, K.; Bricks, J. L.; Slominskii, J. L.; Resch-Genger, U. In *Near-Infrared Dyes for High Technology Applications*; Dähne, S., Resch-Genger, U., Wolfbeis, O. S., Eds.; Kluwer Academic: Dordrecht, The Netherlands, 1998; p 191. Rurack, K.; Resch-Genger, U. *BAM Res. Rep.* **1998**, *223*, 1.

(28) Ishikawa, J.; Sakamoto, H.; Wada, H. *J. Chem. Soc., Perkin Trans. 2* **1999**, 1273.

(29) Clarke, R. J.; Coates, J. H.; Lincoln, S. E. *Inorg. Chim. Acta* **1988**, *153*, 21. Akkaya, E. U.; Huston, M. E.; Czarnik, A. W. *J. Am. Chem. Soc.* **1990**, *112*, 3590. Ghosh, P.; Bharadwaj, P. K.; Mandal, S.; Ghosh, S. *J. Am. Chem. Soc.* **1996**, *118*, 1553. Sclafani, J. A.; Maranto, M. T.; Sisk, T. M.; Van Arman, S. A. *Tetrahedron Lett.* **1996**, *37*, 2193. Schuster, M.; Sandor, M. *Fresenius J. Anal. Chem.* **1996**, *356*, 326. Klonkowski, A. M.; Kledzik, K.; Ossowski, T.; Jankowska-Frydel, A. *J. Mater. Chem.* **1998**, *8*, 1245. Ramachandram, B.; Samanta, A. *J. Phys. Chem. A* **1998**, *102*, 10579. Winkler, J. D.; Bowen, C. M.; Michelet, V. *J. Am. Chem. Soc.* **1998**, *120*, 3237. Sandor, M.; Geistmann, F.; Schuster, M. *Anal. Chim. Acta* **1999**, *388*, 19. Ishikawa, J.; Sakamoto, H.; Nakao, S.; Wada, H. *J. Org. Chem.* **1999**, *64*, 1913. Hennrich, G.; Sonnenschein, H.; Resch-Genger, U. *J. Am. Chem. Soc.* **1999**, *121*, 5073.

(30) Fabbrizzi, L.; Licchelli, M.; Pallavicini, P.; Perotti, A.; Taglietti, A.; Sacchi, D. *Chem.-Eur. J.* **1996**, *2*, 75.

(31) De Santis, G.; Fabbrizzi, L.; Licchelli, M.; Mangano, C.; Sacchi, D.; Sardone, N. *Inorg. Chim. Acta* **1997**, *257*, 69.

(32) Pearson, R. G. *J. Am. Chem. Soc.* **1963**, *85*, 3533.

(33) Pearson, R. G. *Inorg. Chem.* **1988**, *27*, 734.

(34) Anderegg, G. *Helv. Chim. Acta* **1981**, *64*, 1790. Luboch, E.; Cygan, A.; Biernat, J. F. *Inorg. Chim. Acta* **1983**, *68*, 201. Arnaud-Neu, F.; Yahya, R.; Schwing-Weill, M.-J. *J. Chim. Phys. Phys.-Chim. Biol.* **1986**, *83*, 403.

(35) Lindoy, L. F. In *Cation Binding by Macrocycles*; Inoue, Y., Gokel, G. W., Eds.; Marcel Dekker: New York, 1990; p 599.

(36) Saito, K.; Masuda, Y.; Sekido, E. *Anal. Chim. Acta* **1983**, *151*, 447.

(37) Sakamoto, H.; Ishikawa, J.; Mizuno, T.; Doi, K.; Otomo, M. *Chem. Lett.* **1993**, 609. Sakamoto, H.; Ishikawa, J.; Otomo, M. *Bull. Chem. Soc. Jpn.* **1995**, *68*, 2831.

(38) McClure, D. S. *J. Chem. Phys.* **1952**, *20*, 682. Robinson, G. W. *J. Chem. Phys.* **1967**, *46*, 572.

(39) Varnes, A. W.; Dodson, R. B.; Wehry, E. L. *J. Am. Chem. Soc.* **1972**, *94*, 946.

(40) Masuhara, H.; Shioyama, H.; Saito, T.; Hamada, K.; Yasoshima, S.; Mataga, N. *J. Phys. Chem.* **1984**, *88*, 5868.

(41) Von Kostanecki, S.; Tambor, J. *Chem. Ber.* **1899**, *32*, 1921.

(42) Woolenweber, E.; Jay, M.; Favre-Bonvin, J. *Phytochemistry* **1974**, *13*, 2618. Saitoh, T.; Shibata, S. *Tetrahedron Lett.* **1975**, 4461. Nagarajan, G. R.; Parmer, V. S. *Phytochemistry* **1977**, *16*, 1317. Malterud, K. E.; Anthonsen, T.; Lorentzen, G. B. *Phytochemistry* **1977**, *16*, 1805.

(43) Stecher, H. *Adhesion* **1958**, *2*, 243.

(44) Schellenberg, W. D.; Heinz, J. Farbenfabriken Bayer Akt. Ges. German Patent 1039835 1959; *Chem. Abstr.* **1961**, *55*, 7119f. Monroe, B.; Smothers, W. K.; Keys, D. E.; Krebs, R. R.; Mickish, D. J.; Harrington, A. F.; Schicker, S. R.; Armstrong, M. K.; Chan, D. M. T.; Weathers, C. I. *J. Imaging Sci.* **1991**, *35*, 19. Su, G.-B.; He, Y.-P.; Li, Z.-D. *Jiegou Huaxue (Chinese J. Struct. Chem., Engl. Transl.)* **1997**, *16*, 263. Mager, L.; Melzer, C.; Barzoukas, M.; Fort, A.; Mery, S.; Nicoud, J.-F. *Appl. Phys. Lett.* **1997**, *71*, 2248.

(45) Linke, H. A. B.; Eveleigh, D. E. *Z. Naturforsch.* **1975**, *30b*, 740. Horowitz, R. M.; Gentili, B. U.S. Patent 3890298, 1975; *Chem. Abstr.* **1975**, *83*, 147706g.

(46) Geiger, W. B.; Conn, J. E. *J. Am. Chem. Soc.* **1945**, *67*, 112. Schraufstätter, E.; Deutsch, S. *Z. Naturforsch.* **1949**, *4b*, 276. Pachmann, A. N.; Rublin, N. *Am. J. Pharm.* **1962**, *134*, 45. Stenlid, G. *Physiol. Plant.* **1968**, *21*, 882.

(47) Szmant, H. H.; Basso, A. J. *J. Am. Chem. Soc.* **1952**, *74*, 4397.

(48) Tsukerman, S. V.; Maslennikova, V. P.; Lavruskin, V. F. *Opt. Spectrosc.* **1967**, *23*, 213.

(49) Nikitina, A. N.; Fedyunina, G. M.; Umirzakov, B.; Yanovskaya, L. A.; Kucherov, V. F. *Opt. Spectrosc.* **1973**, *34*, 163.

(50) Nicodem, D. E.; de M. G. Matos, J. A. *J. Photochem.* **1981**, *15*, 193.
(51) Caldwell, R. A.; Singh, M. *J. Am. Chem. Soc.* **1983**, *105*, 5139.
(52) Wang, Y. *J. Phys. Chem.* **1985**, *89*, 3799.
(53) Eisenhart, J. M.; Ellis, A. B. *J. Org. Chem.* **1985**, *50*, 4108.
(54) Gustav, K.; Bartsch, U.; Karnizschky, K. *Z. Chem.* **1989**, *29*, 213.
(55) DeVoe, R. J.; Sahyun, M. R. V.; Schmidt, E.; Sadrai, M.; Serpone, N.; Sharma, D. K. *Can. J. Chem.* **1989**, *67*, 1565.
(56) Wang, P.-F.; Wu, S.-K. *Acta Chim. Sin.* **1994**, *52*, 341.
(57) Wang, P.; Wu, S. *J. Photochem. Photobiol. A: Chem.* **1995**, *86*, 109.
(58) Stobbe, H.; Bremer, K. *J. prakt. Chem.* **1929**, *123*, 1. Dhar, D. N.; Singhal, D. V. *Spectrochim. Acta* **1970**, *26A*, 1171. Ebied, E.-Z. M.; Abdel-Kader, M. H.; Issa, R. M.; El-Daly, S. A. *Chem. Phys. Lett.* **1988**, *146*, 331. El-Daly, S. A.; Ebied, E.-Z. M. *Spectrochim. Acta* **1994**, *50A*, 1227. Jiang, Y.-B.; Wang, X.-J.; Lin, L. *J. Phys. Chem.* **1994**, *98*, 12367. Jiang, Y.-B.; Wang, X.-J. *J. Photochem. Photobiol. A: Chem.* **1994**, *81*, 205. Itoh, H.; Takada, A.; Kudo, H.; Yokoyama, H.; Senda, Y.; Urano, T.; Nagasaka, H. *Bull. Chem. Soc. Jpn.* **1997**, *70*, 2221. Iwata, S.; Nishino, T.; Inoue, H.; Nagata, N.; Satomi, Y.; Nishino, H.; Shibata, S. *Biol. Pharm. Bull.* **1997**, *20*, 1266.
(59) Throughout the Experimental Section and the Results and Discussion, additional information is provided in the Supporting Information where the corresponding sections are numbered consecutively starting with S1.
(60) *Gmelins Handbuch der Anorganischen Chemie. Chlor.*, 8th ed.; VCH: Berlin, 1927.
(61) The setup employed in the temperature-dependent measurements is given in the Supporting Information, section S2.
(62) Olmsted, J., III *J. Phys. Chem.* **1979**, *83*, 2581. Demas, J. N. In *Optical Radiation Measurements*; Mielenz, K. D., Ed.; Academic: New York, 1982; Vol. 3, p 195. Drexhage, K. H. *J. Res. Natl. Bur. Stand.* **1976**, *80A*, 421. Drake, J. M.; Lesiecki, M. L.; Camaioni, D. M. *Chem. Phys. Lett.* **1985**, *113*, 530.
(63) Resch, U.; Rurack, K. *Proc. SPIE-Int. Soc. Opt. Eng.* **1997**, *3105*, 96.
(64) A prerequisite for any structural statement on the complexes is the unequivocal assignment of the signals for the free chalcones. The alternating electron density between the carbonyl and DMA group, the characteristic splitting of the signals of the CH-α and CH-β group ($^3J_{\alpha,\beta}^{\text{trans}} = 16$ Hz) and the AA′XX′ system of the aromatic ortho and meta protons facilitated this assignment. In the case of the heterocyclic acceptors benzothaizole and quinoline, additional COSY spectra were recorded, and for the quinoline system, long-range coupling ^5J of the protons H-4 and H-8 induced a cross-peak. Thus, definite assignment of the signals was possible in all cases and coupling constants as well as splitting patterns found correlate well with literature data (Pretsch, E.; Clerc, T.; Seibl, J.; Simon, W. *Tables of Spectral Data for Structure Determination of Organic Compounds*; Springer: Berlin, 1989; pp H330, H335.).
(65) Fery-Forgues, S.; Le Bris, M. T.; Guetté, J.-P.; Valeur, B. *J. Phys. Chem.* **1988**, *92*, 6233.
(66) The conductometric experiments are described in the Supporting Information, section S5.
(67) The X-ray structure data of the compounds investigated have been deposited at the Cambridge Crystallographic Data Centre, 12 Union Road, Cambridge CB2 1EZ, U.K., and the six compounds have been allocated the deposition numbers CCDC 132989−CCDC 132994. The crystal data are provided in the Supporting Information, section S6.
(68) Jonker, S. A. Ph.D. Thesis, University of Amsterdam, Amsterdam, 1989.
(69) Complexes of MAP-A15C5-1: Zoutberg, M. C.; Reiss, C. A.; Goubitz, K.; Heijdenrijk, D. *Acta Crystallogr.* **1989**, *C45*, 1359. Kronenburg, M. J.; Reiss, C. A.; Goubitz, K.; Heijdenrijk, D. *Acta Crystallogr.* **1989**, *C45*, 1361. Complexes of MAP-A15C5-2: Häming, L. P.; Reiss, C. A.; Goubitz, K.; Heijdenrijk, D. *Acta Crystallogr.* **1990**, *C46*, 462. Reiss, C. A.; Goubitz, K.; Heijdenrijk, D. *Acta Crystallogr.* **1990**, *C46*, 1089. Free dyes: Goubitz, K.; Reiss, C. A.; Heijdenrijk, D. *Acta Crystallogr.* **1989**, *C45*, 1356. Reiss, C. A.; Goubitz, K.; Zoutberg, M. C.; Heijdenrijk, D. *Acta Crystallogr.* **1989**, *C45*, 1366.
(70) Ishikawa, J.; Sakamoto, H.; Mizuno, T.; Otomo, M. *Bull. Chem. Soc. Jpn.* **1995**, *68*, 3071.
(71) Liptay, W. *Z. Naturforsch.* **1965**, *20a*, 1441.
(72) Lippert, E. *Z. Naturforsch.* **1955**, *10a*, 541.
(73) A second component of minor significance was observed but could not be verified any further with the simple method employed.
(74) Lippert, E. *Z. Elektrochem.* **1957**, *61*, 962. Mataga, N.; Kaifu, Y.; Koizumi, M. *Bull. Chem. Soc. Jpn.* **1956**, *29*, 465.
(75) The Onsager radii were taken to $a_O = 6.4$ Å (**1a**), 7.3 Å (**1c**), 6.5 Å (**1e**), 5.7 Å (**2a**), 6.2 Å (**3**) on the basis of X-ray data (see Supporting Information, section S7), and the ground-state dipole moments, obtained from the optimized geometry in the ground state by semiempirical calculations, to $\mu_{gs} = 2.9$ D (**1a**), 4.6 D (**1c**), 4.3 D (**1e**), 3.9 D (**2a**), 2.6 D (**3**) (see section S7).
(76) Dimroth, K.; Reichardt, C.; Siepmann, T.; Bohlmann, F. *Justsus Liebigs Ann. Chem.* **1963**, *661*, 1. Catalán, J.; López, V.; Pérez, P.; Martín-Villamil, R.; Rodríguez, J.-G. *Liebigs Ann.* **1995**, 241. Catalán, J. *J. Org. Chem.* **1995**, *60*, 8315.
(77) Whereas the Lippert−Mataga formalism relies only on physical properties of the solvent and often leads to poor correlations for solvents that cannot be adequately modeled by a continuum dielectric description, the empirical solvent polarity scales were derived from the solvatochromic behavior of a certain polar dye molecule that "does not know" if a solvent is apolar or not. Thus, the polarity scales are often more precise in accounting for effects such as solvent repolarization.[78]
(78) Reynolds, L.; Gardecki, J. A.; Frankland, S. J. V.; Horng, M. L.; Maroncelli, M. *J. Phys. Chem.* **1996**, *100*, 10337.
(79) Rurack, K.; Dekhtyar, M. L.; Bricks, J. L.; Resch-Genger, U.; Rettig, W. *J. Phys. Chem. A.*, **1999**, *103*, 9626.
(80) Fery-Forgues, S.; Le Bris, M. T.; Mialocq, J.-C.; Pouget, J.; Rettig, W.; Valeur, B. *J. Phys. Chem.* **1992**, *96*, 701.
(81) Lehn, J.-M. *Struct. Bonding (Berlin)* **1973**, *16*, 1.
(82) Kosower, E. M. *Acc. Chem. Res.* **1982**, *15*, 259.
(83) Rettig, W. *Top. Curr. Chem.* **1994**, *169*, 253.
(84) Strehmel, B.; Seifert, H.; Rettig, W. *J. Phys. Chem. B* **1997**, *101*, 2232.
(85) Birks, J. B. *Photophysics of Aromatic Molecules*; Wiley: London, 1970. Löfroth, J.-E. *J. Phys. Chem.* **1986**, *90*, 1160. Leinhos, U.; Kühnle, W.; Zachariasse, K. A. *J. Phys. Chem.* **1991**, *95*, 2013. Schuddeboom, W.; Jonker, S. A.; Warman, J. M.; Leinhos, U.; Kühnle, W.; Zachariasse, K. A. *J. Phys. Chem.* **1992**, *96*, 10809.
(86) A similar decay behavior has been found for **1b** in polar solvents, only slightly solvent polarity-dependent, yielding a fast decay component of 30−200 ps and a slow decay component of ca. 1.6 ns (a_{rel} ca. 0.6), both with positive amplitudes throughout the whole emission range measured.
(87) Braun, D.; Rettig, W. *Chem. Phys. Lett.* **1997**, *268*, 110.
(88) The rate constants of radiative k_f and nonradiative k_{nr} deactivation are generally given by $k_f = \phi_f/\tau_f$ and $k_{nr} = (1 - \phi_f)/\tau_f$.
(89) Maroncelli, M.; Fleming, G. R. *J. Chem. Phys.* **1987**, *86*, 6221.
(90) Horng, M. L.; Gardecki, J. A.; Papazyan, A.; Maroncelli, M. *J. Phys. Chem.* **1995**, *99*, 17311.
(91) Su, S.-G.; Simon, J. D. *J. Phys. Chem.* **1987**, *91*, 2693.
(92) Simon, J. D. *Acc. Chem. Res.* **1988**, *21*, 128.
(93) Declémy, A.; Rullière, C.; Kottis, P. *Laser Chem.* **1990**, *10*, 413.
(94) Note that for a series of highly fluorescent coumarin dyes, Gustavsson et al. observed spectral response functions with largely varying τ_i of 1.05−3.36 ps (short) and τ_i of 11.17−20.13 ps (longer lived decay component in methanol) for the different dyes employed.[95]
(95) Gustavsson, T.; Cassara, L.; Gulbinas, V.; Gurzadyan, G.; Mialocq, J.-C.; Pommeret, S.; Sorgius, M.; van der Meulen, P. *J. Phys. Chem. A* **1998**, *102*, 4229.
(96) The spectral response function for following solvation dynamics, eq 9, is obtained from log-normal fits of TRES and include the peak frequency $\nu_p(t)$ and the average frequency of the spectrum, $\bar{\nu}(t) = \nu_p(t) + (w(t)/2\gamma(t))[\exp(3\gamma(t)^2/4 \ln 2) - 1]$. Here, w is the width and γ the asymmetry of the fitted time trace spectrum (see refs 78, 89, and 90, and: Fee, R. S.; Maroncelli, M. *Chem. Phys.* **1994**, *183*, 235.). The correlation function $C_\nu(t)$ (eq 9) is fitted to a sum of exponentials $C_\nu(t) = \sum_i a_i e^{-t(\tau_i)^{-1}}$ with $a_i \geq 0$ and $\sum_i a_i = 1$ and the single components are related to $\langle\tau\rangle$ according to $\langle\tau\rangle = \sum_i a_i \tau_i$.
(97) Kahlow, M. A.; Kang, T. J.; Barbara, P. F. *J. Phys. Chem.* **1987**, *91*, 6452. Pöllinger, F.; Heitele, H.; Michel-Beyerle, M. E.; Anders, C.; Futscher, M.; Staab, H. A. *Chem. Phys. Lett.* **1992**, *198*, 645. Rossky, P. J.; Simon, J. D. *Nature* **1994**, *370*, 263.
(98) The occurrence of trans−cis isomerization in the ground state was excluded by recording the emission spectra of **1a** and **1c** as a function of laser excitation energy up to 10 mW (continuous wave). Furthermore, HPLC analysis with UV/vis diode array detection of irradiated samples of **1a** and **1c** showed only one peak, its absorption spectrum being identical to that of a reference sample kept in the dark. Chalcone cis isomers described in the literature so far show a strongly hypsochromically shifted absorption spectrum.[50]
(99) Saltiel, J.; Sun, Y.-P. In *Photochromism*; Dürr, H., Bouas-Laurent, H., Eds.; Elsevier: Amsterdam, 1990; p 64.
(100) Rabinovich, D. *J. Chem. Soc. B* **1970**, 11. Jungk, A. E.; Schmidt, G. M. J. *J. Chem. Soc. B* **1970**, 1427. Rabinovich, D.; Schmidt, G. M. J.; Shakked, Z. *J. Chem. Soc., Perkin Trans. 2* **1973**, 33.
(101) Tsukerman, S. V.; Izvekov, V. P.; Lavrushin, V. F. *Zh. Fiz. Khim.* **1968**, *42*, 2159. Tsukerman, S. V.; Orlov, V. D.; Lam, N. T.; Lavrushin, V. F. *Khim. Geterotsikl. Soedin.* **1969**, *6*, 974. Orlov, V. D.; Tsukerman, S. V.; Lavrushin, V. F. *Vop. Stereokhim.* **1971**, *1*, 89.
(102) Hayes, W. P.; Timmons, C. J. *Spectrochim. Acta* **1968**, *24A*, 323.
(103) Rettig, W.; Majenz, W.; Herter, R.; Létard, J.-F.; Lapouyade, R. *Pure Appl. Chem.* **1993**, *65*, 1699.
(104) Wassam, W. A., Jr.; Lim, E. C. *J. Chem. Phys.* **1978**, *68*, 433.
(105) Létard, J.-F.; Lapouyade, R.; Rettig, W. *J. Am. Chem. Soc.* **1993**, *115*, 2441.

(106) Siebrand, W. *J. Chem. Phys.* **1967**, *46*, 440. Siebrand, W. *J. Phys. Chem.* **1967**, *47*, 2441.

(107) Martin, M. M.; Ikeda, N.; Okada, T.; Mataga, N. *J. Phys. Chem.* **1982**, *86*, 4148. Itoh, M.; Adachi, T.; Tokumura, K. *J. Am. Chem. Soc.* **1984**, *106*, 850.

(108) See, for instance, a compound with A = phenyl (Scheme 1) and D = OCH_3 [49,54] as well as a derivative with A = 4-O_2N-phenyl and D = H.[54] The same accounts for derivatives with a reversed A−D-substitution pattern such as 4-$(H_3C)_2$N-phenyl and 4′-Cl[54] or 4-$(H_3C)_2$N-phenyl and 4′-NO_2.[54] Additionally, symmetrical D−A−D-chalcones of the 1,5-diphenyl-1,4-pentadien-3-one type with amino donor groups are again fluorescent.[53,55.]

(109) At higher excess of Hg^{II} in the solution, quenching is observed. Whether a diffusion controlled process (typically observed for "heavy atoms" in a solution containing a fluorescent dye) plays a significant role is not yet clear since the formation of another chelate-like complex at higher ion concentrations might as well interfere (see discussion in section 3.10).

(110) For Hg^{II}, these complexes are only well-defined in terms of steady-state spectroscopy (see discussion in section 3.10).

(111) Note that employing a fourth decay component is possible but does not significantly improve the fit (see discussion in section 3.8).

(112) Interestingly, such effects were not observed for **1d** and Mg^{II} in the millimolar concentration range.

(113) Dähne, S. *Science* **1978**, *199*, 1163. Dähne, S. *Chimia* **1994**, *45*, 104;.

(114) Kachkovski, A. D.; Dyadyusha, G. G.; Dekhtyar, M. L. *Dyes Pigm.* **1991**, *15*, 191.

(115) Druzhinin, S. I.; Rusalov, M. V.; Uzhinov, B. M.; Gromov, S. P.; Sergeev, S. A.; Alfimov, M. V. *J. Fluoresc.* **1999**, *9*, 33.

(116) The decay associated spectra ($DAS_i(\lambda)$) are given by $DAS_i(\lambda) = a_i(\lambda)F_{SS}^{tot}(\lambda)/\sum_i a_i(\lambda)\tau_i$ with $a_i(\lambda)$ the amplitude of decay component i and $F_{SS}^{tot}(\lambda)$ the normalized steady-state fluorescence intensity.[84,85] Depending on the excited-state reaction model, the species associated spectra ($SAS_i(\lambda)$) can be obtained from the decay times and $DAS_i(\lambda)$ according to various formalisms described in the literature.[84] Extrapolation of the $SAS_i(\lambda)$ ratios into the high- and low-energy regions of the spectrum further allows us to check the validity of the formalism employed, i.e., the reaction model anticipated.

(117) As described in section 3.1, **1d** is present in two conformations even in the solid state. Unfortunately, we were not able to prepare an X-ray sample of **1d**⊂Hg^{II}.

(118) Nieboer, E.; Richardson, D. H. S. *Environ. Pollut. Ser. B* **1980**, *1*, 3.

(119) Lamb, J. D.; Izatt, R. M.; Swain, C. S.; Christensen, J. J. *J. Am. Chem. Soc.* **1980**, *102*, 475. Poonia, N. S.; Bajaj, A. V. *Chem. Rev.* **1979**, *79*, 389.

(120) Shannon, R. D. *Acta Crystallogr.* **1976**, *32A*, 751.

(121) Iwachido, T.; Minami, M.; Kimura, M.; Sadakane, A.; Kawasaki, M.; Toei, K. *Bull. Chem. Soc. Jpn.* **1980**, *53*, 703.

(122) Fery-Forgues, S.; Bourson, J.; Dallery, L.; Valeur, B. *New J. Chem.* **1990**, *14*, 617.

(123) Riesen, P. C.; Kaden, T. A. *Helv. Chim. Acta* **1995**, *78*, 1325.

(124) Frensdorff, H. K. *J. Am. Chem. Soc.* **1971**, *93*, 600.

(125) Accordingly, the addition of Ag^I to **1c**, even at a high excess, does not yield any measurable spectral changes. Létard et al. described similar effects for the complexation of Ag^I to DCS-A15C5 (Scheme 2) in acetonitrile.[17] Even for lariat ethers, where a methylene spacer between the phenyl ring and the A15C5 receptor allows for an encapsulation of Ag^I, the complex stability constants in acetonitrile reported for Li^I and Na^I were at least 10 and at most 100 times higher than those reported for Ag^I.[126] Strong coordination of Ag^I ions by solvent molecules are the main reason for this behavior in acetonitrile.[127]

(126) Gustowski, D. A.; Gatto, V. J.; Mallen, Echegoyen, L.; Gokel, G. W. *J. Org. Chem.* **1987**, *52*, 5172.

(127) Buschmann, H.-J. *J. Solut. Chem.* **1988**, *17*, 277. Burchard, T.; Cox, B. G.; Firman, P.; Schneider, H. *Ber. Bunsen-Ges. Phys. Chem.* **1994**, *98*, 1526.

(128) Lednev, I. K.; Ye, T.-Q.; Hester, R. E.; Moore, J. N. *J. Phys. Chem.* **1997**, *101*, 4966. Thomas, K. J.; Thomas, K. G.; Manojkumar, T. K.; Das, S.; George, M. V. *Proc. Indian Acad. Sci. (Chem. Sci.)* **1994**, *106*, 1375.

(129) Soroka, K.; Vithanage, R. S.; Phillips, D. A.; Walker, B.; Dasgupta, P. K. *Anal. Chem.* **1987**, *59*, 629.

(130) Hancock, R. D.; Martell, A. E. *Chem. Rev.* **1989**, *89*, 1875.

(131) Roshal, A. D.; Grigorovich, A. V.; Doroshenko, A. O.; Pivovarenko, V. G.; Demchenko, A. P. *J. Phys. Chem. A* **1998**, *102*, 5907.

(132) Marcotte, N.; Fery-Forgues, S.; Lavabre, D.; Marguet, S.; Pivovarenko, V. G. *J. Phys. Chem. A* **1999**, *103*, 3163.

(133) Lytle, F. E. *Appl. Spectrosc.* **1970**, *24*, 319.

(134) In the case of **1a** and Hg^{II}, analysis of the titration spectra given in Figure 15 yielded acceptable fits for a 1:1 model (according to eq 5) with a log K_S of 5.0.

(135) $a_{rel}(3) = a(3)/(a(2) + a(3))$ with the 0.5 ns (1.1 ns) decay component as species 2 (3).

(136) Note that excitation between 330 and 370 nm was not possible with the instrumental setup employed, thus limiting fluorescence decay studies as a function of excitation wavelength to a great extent in this case. In the experiments reported here, no pronounced trends in the relative amplitudes of the decay components were observed. Furthermore, the lifetimes are similar (within experimental error) for both $x_{M/L}$.

(137) The spectra were fitted with multiple Gaussian peak functions and the molar absorptivities were only roughly determined by fitting two spectra: (s) denotes strong (>5000 M^{-1} cm^{-1}), (m) medium (5000 M^{-1} $cm^{-1} > x >$ 1000 M^{-1} cm^{-1}), and (w) weak bands (<1000 M^{-1} cm^{-1}); "$\epsilon \sim$ xy" indicates determination from two measurements for nonoverlapping or weakly overlapping bands.

(138) Westerby, B. C.; Juntunen, K. L.; Leggett, G. H.; Pett, V. B.; Koenigbauer, M. J.; Purgett, M. D.; Taschner, M. J.; Ochrymowycz, L. A.; Rorabacher, D. B. *Inorg. Chem.* **1991**, *30*, 2109.

(139) At 24 100 cm^{-1} (ϵ = 8000 M^{-1} cm^{-1}, $T_4$15C5; ϵ = 7000 M^{-1} cm^{-1}, $T_5$15C5),[140] 27 400 cm^{-1} (ϵ = 6000 M^{-1} cm^{-1}, $AT_3$14C4),[138] 25 500 cm^{-1} (ϵ = 2500 M^{-1} cm^{-1}, $A_2T_4$18C6),[141] and the weaker transitions at 17 700 cm^{-1} (ϵ = 1100 M^{-1} cm^{-1}, $T_4$15C5;[140] ϵ = 2000 M^{-1} cm^{-1}, T_5-15C5),[140] 18 200 cm^{-1} (ϵ = 1000 M^{-1} cm^{-1}, $AT_3$14C4),[138] and 16 300 cm^{-1} (ϵ = 202 M^{-1} cm^{-1}, $A_2T_4$18C6).[141]

(140) Jones, T. E.; Rorabacher, D. B.; Ochrymowycz, L. A. *J. Am. Chem. Soc.* **1975**, *97*, 7485.

(141) Atkinson, N.; Blake, A. J.; Drew, M. G. B.; Forsyth, G.; Gould, R. O.; Lavery, A. J.; Reid, G.; Schröder, M. *J. Chem. Soc., Dalton Trans.* **1992**, 2993.

(142) Due to the small overlap between sulfur π-orbitals and Cu^{II} d-orbitals, π(S) → Cu LMCT transitions are generally weaker than σ(S) → Cu LMCT transitions.[143]

(143) Nikles, D. E.; Anderson, A. B.; Urbach, F. L. In *Copper Coordination Chemistry: Biochemical and Inorganic Perspectives*; Karlin, K. D., Zubieta, J., Eds.; Adenine: New York, 1983; p 203.

(144) Schugar, H. J. In *Copper Coordination Chemistry: Biochemical and Inorganic Perspectives*; Karlin, K. D., Zubieta, J., Eds.; Adenine: New York, 1983; p 43. Amundsen, A. R.; Whelan, J.; Bosnich, B. *J. Am. Chem. Soc.* **1977**, *99*, 6730.

(145) Note that these regions are not defined by sharp isosbestic points, indicating mixed complex formation.

(146) For Ph-A15C5 and **2a**, bands of comparatively intensity are found at 20 900 cm^{-1} (Ph-A15C5⊂Cu^{II}) and 21 200 cm^{-1} (**2a**⊂Cu^{II}), respectively, suggesting coordination to the anilino nitrogen atom.

(147) Kaden, T. A.; Kaderli, S.; Sager, W.; Siegfried-Hertli, L. C.; Zuberbühler, A. D. *Helv. Chim. Acta* **1986**, *69*, 1216.

(148) Rorabacher, D. B.; Martin, M. J.; Koenigbauer, M. J.; Malik, M.; Schroeder, R. R.; Endicott, J. F.; Ochrymowycz, L. A. In *Copper Coordination Chemistry: Biochemical and Inorganic Perspectives*; Karlin, K. D., Zubieta, J., Eds.; Adenine: New York, 1983; p 167.

(149) Corfield, P. W. R.; Ceccarelli, C.; Glick, M. D.; Moy, I. W.-Y.; Ochrymowycz, L. A.; Rorabacher, D. B. *J. Am. Chem. Soc.* **1985**, *107*, 2399.

(150) The shifts observed for Ag^I are already comparatively small (Table 3).

(151) Fujisawa, K.; Imai, S.; Kitajima, N.; Moro-oka, Y. *Inorg. Chem.* **1998**, *37*, 168.

(152) Smith, R. M.; Martell, A. E. *Critical Stability Constants Volume 2: Amines*; Plenum: New York, 1975; Vol. 2, p 36.

(153) Lindoy, L. F.; Lip, H. C.; Rea, J. H.; Smith, R. J.; Henrick, K.; McPartlin, M.; Tasker, P. A. *Inorg. Chem.* **1980**, *19*, 3360.

(154) Izatt, R. M.; Terry, R. E.; Hansen, L. D.; Avondet, A. G.; Bradshaw, J. S.; Dalley, N. K.; Jensen, T. E.; Christensen, J. J.; Haymore, B. L. *Inorg. Chim. Acta* **1978**, *30*, 1.

(155) Lindoy, L. F. In *Synthesis of Macrocycles*; Izatt, R. M.; Christensen, J. J., Eds.; John Wiley & Sons: New York, 1987; p 53.

(156) Adam, K. R.; Baldwin, D. S.; Bashall, A.; Lindoy, L. F.; McPartlin, M.; Powell, H. R. *J. Chem. Soc., Dalton Trans.* **1994**, 237.

(157) Rurack, K.; Resch-Genger, U.; Rettig, W. *J. Photochem. Photobiol. A: Chem.* **1998**, *118*, 143.

(158) Jonusaukas, G.; Lapouyade, R.; Delmond, S.; Létard, J. F.; Rullière, C. *J. Chim. Phys. Phys.-Chim. Biol.* **1996**, *93*, 1670.

(159) Cox, B. G.; Garcia-Rosas, J.; Schneider, H. *J. Am. Chem. Soc.* **1981**, *103*, 1384.

(160) Heitsch, H.; Wagner, A.; Schölkens, B. A.; Wirth, K. *Bioorg. Med. Chem. Lett.* **1999**, *9*, 327.

(161) Bourson, J.; Borrel, M.-N.; Valeur, B. *Anal. Chim. Acta* **1992**, *257*, 189.

(162) The remaining absorption at ca. 22 000 cm^{-1} (shoulder) at large excess of metal ion is attributed to uncomplexed dye molecules in the equilibrated state. Similar effects have been described for other ICT probes.[18,163] Mateeva et al. discussed nπ* transitions being responsible for these bands but this assumption could not be supported here.[18]

(163) Cazaux, L.; Faher, M.; Lopez, A.; Picard, C.; Tisnes, P. *J. Photochem. Photobiol. A: Chem.* **1994**, *77*, 217.

(164) Due to the heterocyclic donor atoms being present in the chromophore (and in form of the nitrogen in the receptor), at higher concentrations, i.e., at $x_{M/L} > 100$, slight spectroscopic changes are observable for other heavy and transition metal ions such as, e.g., Ni^{II} as well. However, the occurrence of these trace metal ions at such concentrations is barely found in matrixes where fluorescence sensing is commonly employed.

(165) Jonker, S. A.; Verhoeven, J. W.; Reiss, C. A.; Goubitz, K.; Heijdenrijk, D. *Recl. Trav. Chim. Pays-Bas* **1990**, *109*, 154.

(166) Pauling, L. *J. Am. Chem. Soc.* **1927**, *49*, 765.

(167) Hinze, J. *Fortschr. Chem. Forsch.* **1968**, *9*, 448.

(168) Allred, A. L. *J. Inorg. Nucl. Chem.* **1961**, *17*, 215. Allred, A. L.; Rochow, E. G- *J. Inorg. Nucl. Chem.* **1958**, *5*, 264.

(169) Dalley, N. K. In *Synthetic Multidentate Macrocyclic Compounds*; Izatt, R. M., Christensen, J. J., Eds.; Academic: New York, 1978; p 207.